Article

Phytochemical Profiling, Antioxidant and Cognitive-Enhancing Effect of *Helichrysum italicum* ssp. *italicum* (Roth) G. Don (Asteraceae)

Reneta Gevrenova [1], **Ivanka Kostadinova** [2], **Alexandra Stefanova** [2], **Vessela Balabanova** [1], **Gokhan Zengin** [3], **Dimitrina Zheleva-Dimitrova** [1,*] **and Georgi Momekov** [2]

[1] Department of Pharmacognosy, Faculty of Pharmacy, Medical University, 1000 Sofia, Bulgaria; rgevrenova@pharmfac.mu-sofia.bg (R.G.); vbalabanova@pharmfac.mu-sofia.bg (V.B.)

[2] Department of Pharmacology, Pharmacotherapy, and Toxicology, Faculty of Pharmacy, Medical University, 1000 Sofia, Bulgaria; i.kostadinova@pharmfac.mu-sofia.bg (I.K.); astefanova22@gmail.com (A.S.); gmomekov@pharmfac.mu-sofia.bg (G.M.)

[3] Physiology and Biochemistry Research Laboratory, Department of Biology, Science Faculty, Selcuk University, Konya 42130, Turkey; gokhanzengin@selcuk.edu.tr

* Correspondence: dzheleva@pharmfac.mu-sofia.bg

Abstract: This study aimed at the evaluation of the antioxidant and cognitive-enhancing effect of methanol–aqueous extract from *Helichrysum italicum* ssp. *italicum* aerial parts. Significant radical scavenging activity (110.33 ± 3.47 and 234.70 ± 5.21 mg TE/g for DPPH and ABTS) and reducing power (354.23 ± 17.51 and 210.24 ± 8.68 mg TE/g for CUPRAC and FRAP) were observed. The extract showed average acetylcholinesterase and low butyrylcholinesterase inhibitory potential. *H. italicum* extract (200 mg/kg/po) administered in combination with galantamine (3 mg/kg/po) for 12 days significantly improved the memory and learning process compared with galantamine alone in the passive avoidance test. The effect was comparable to that of *Ginkgo biloba* extract (100 mg/kg/po). In deep secondary metabolite annotation of the extract by UHPLC-HRMS, more than 90 hydroxybenzoic and hydroxycinnamic acid-glycosides, phenylethanoid glycosides, a series of acylquinic and caffeoylhexaric acids, methoxylated derivatives of scutellarein, quercetagetin and 6-hydroxyluteolin, and prenylated phloroglucinol-α-pyrones were reported for the first time in *H. italicum*. Fragmentation patterns of four subclasses of heterodimer-pyrones were proposed. In-depth profiling of the pyrones revealed 23 compounds undescribed in the literature. Pyrones and acylphloroglucinols together with acylquinic acids could account for memory improvement. The presented research advanced our knowledge of *H. italicum*, highlighting the species as a rich source of secondary metabolites with cognitive-enhancing potential.

Keywords: *Helichyrsum*; antioxidant; memory function; phenolics; enzyme inhibition

1. Introduction

Helichrysum italicum (Roth) G. Don (curry plant, immortelle) is an aromatic perennial subshrub belonging to the family Asteraceae, subfamily Asteroideae, and tribe Gnaphalieae. The genus *Helichrysum* Mill. comprises approximately 600 species distributed in central Asia, India, Africa, including Madagascar, and the Mediterranean Basin [1]. The genus has a high occurrence in the Mediterranean areas of Europe. Based on the morphological features, genetic variation, and geographical distribution, *Helichrysum italicum* is divided into six subspecies (ssp.): *italicum*, *microphyllum*, *picardii*, *siculum*, *serotinum*, and *tyrrhenicum* [2]. The name of the genus is derived from the Greek words "helios" and "chryos", which mean "sun" and "gold", respectively. This nomenclature is due to the inflorescences of a bright yellow color typical for the taxon [3]. The common name "immortelle" is related to the everlasting flowers that retain their form and color when dried and thus are used in dry bouquets [4].

H. italicum essential oil is wealthy in various terpenes and mono- and sesquiterpenes with high contribution to the biological activity [2,5]. Recently, the chemical composition of the essential oil of flowering aerial parts of *H. italicum* subsp. *italicum* cultivated in central Italy was analyzed by gas chromatography–mass spectrometry. Seventy-eight components were identified and quantified where neryl acetate revealed the largest relative abundance in the composition (15.75% of the oil), followed by *α*-pinene (8.21%), 4,6,9-trimethyl-8-decene-3,5-dione (italidione I) (7.34%), curcumene and *β*-selinene (5.37%), *γ*-curcumene (4.83%), nerol (4.75%), *α*-selinene (4.68%), limonene (4.55%), linalool (4.42%), and 2,4,6,9-tetramethyl-8-decene-3,5-dione (italidione II) (4.26%). As a result, the oil inhibited in vitro collagenase and elastase activities, with IC50 values of 36.99 ± 1.52 and $135.43 \pm 6.32\,\mu g/mL$, respectively [6]. Neryl acetate is also the predominant compound, with amounts from 15.8% (from plants in the stage of early shoots) to 42.5% (in the full flowering period) in the oil from the *H. italicum* subsp. *italicum* growing in Corsica [7]. However, further studies showed that phenolic and oxygenated compounds contributed to the major components. The reported secondary metabolites from the genus can be categorized into six structural types: flavonoids and chalcones, phenolic acids, terpenes and essential oils, pyrones (both homo- and heterodimeric), benzofurans (bitalin esters), and phloroglucinols [8] consisting mainly of two types of substituents, a prenyl/geranyl group and an acyl group. The most common acyl substituents are methyl, isopropyl, and 2-methylbutanoyl. Various phenolic metabolites were previously isolated and identified including flavonoids, acetophenones, phloroglucinols, tremetones, coumarins and coumarates, phenolic acids, and esters, with their derivatives [5]. More than 100 different compounds were formerly reported as part of the *H. italicum* species with prominent biological activities including the following phenolic acids: hydroxycinnamic acids and derivates, caffeic acid and derivates, and isomers of monocaffeoylquinic acids (CQAs), di- or tri-CQAs, and their glucosides and esters; hydroxybenzoic acids, flavonoids, and their glucosides; and pyrone derivates [9]. Some of the most promising and notable bioactive compounds of *H. italicum* are caffeic acid, chlorogenic acid, pinocembrin, quercetin, naringenin, gnaphaliin, luteolin, tiliroside, arzanol, and ursolic acid [10]. High-resolution mass spectrometry (HRMS) coupled with ultra-high-performance liquid chromatography (UHPLC) and data dependent MS/MS analyses provide very valuable information on secondary metabolites for in-depth metabolite annotation studies [11].

Oxidative stress is an imbalance between reactive oxygen species (ROS) generation and antioxidant defense systems, which are implicated in different pathways of injury in the development of various disorders, including neurodegenerative disorders and aging [12]. As antioxidants are substances that are efficient to scavenge ROS and decrease oxidative damage, these compounds have been studied for therapeutic approaches to many different diseases. Moreover, a deficiency of antioxidants such as vitamins C and E has been associated with cognitive disorders [13]. Therefore, many natural products, especially polyphenols with antioxidant properties could be useful in cognitive decline or neurodegenerative diseases such as Alzheimer's disease [14]. Recently, in vitro DPPH and ABTS antioxidant activity of both essential oils and methanolic extracts of herbs and inflorescences of *H. italicum* has been reported [15]. Results revealed that methanolic extract and essential oil obtained from the aerial parts indicated a higher potential than those originating from the inflorescences. The stronger antioxidant potential may be related to the content of phenolics, especially rutin and chlorogenic acid, known as strong antioxidants [15].

H. italicum is commonly used in the traditional medicine with influences on allergies, colds, coughs, skin, inflammation, infections, and sleeplessness [5]. Previous ethnopharmacological surveys showed the use of *H. italicum* related to different respiratory, digestive, and inflammatory conditions. Its effect on skin conditions such as hematoma, scars, and even psoriasis are also investigated [2]. Several surveys documented the potential use and influence of *H. italicum* on obesity, metabolic syndrome, and type 2 diabetes mellitus. Additionally, clinical data revealed that *H. italicum* subsp. *italicum* infusion acutely

increased the fat oxidation and resting energy expenditure and induced the metabolic effects [16]. A clinical trial investigated the result of *H. italicum* essential oil on mental exhaustion and moderated burnout and revealed a reduction in the perceived level of mental fatigue/burnout [17].

Despite the extensive investigation of the chemical composition and biological activities, there are limited data on the ability of *H. italicum* extracts to improve memory and learning. Hence, the aim of this study was to analyze the secondary metabolites in *H. italicum* var. *italicum*, in the light of its antioxidant and cognitive-enhancing effect. In addition, we hypothesized that the improvement of the learning and memory processes of *H. italicum* methanol–water extract could be attributed to its powerful antioxidant and moderate acetylcholinesterase inhibitory activity.

2. Results and Discussion

A flow chart for the design of the experiment was presented in Figure 1. *H. italicum* aerial parts were extracted with 80% methanol and lyophilized. The dissolved lyophilized extract was first injected in UHPLC-HRMS. Data were acquired using the data-dependent acquisition mode and then converted through a MZmine 2.53 software processing. After obtaining the UHPLC-HRMS profiling, in negative and positive ion modes, extracted chromatograms and their MS/MS spectra followed. Based on the literature data, using the taxonomy as a filter and comparing it with authentic standards, dereplication/annotation of the peaks was carried out. In parallel, spectrophotometric assays were conducted to determine antioxidant and cholinesterase inhibitory potential. Finally, the cognitive-enhancing effect was determined using an in vivo passive avoidance test.
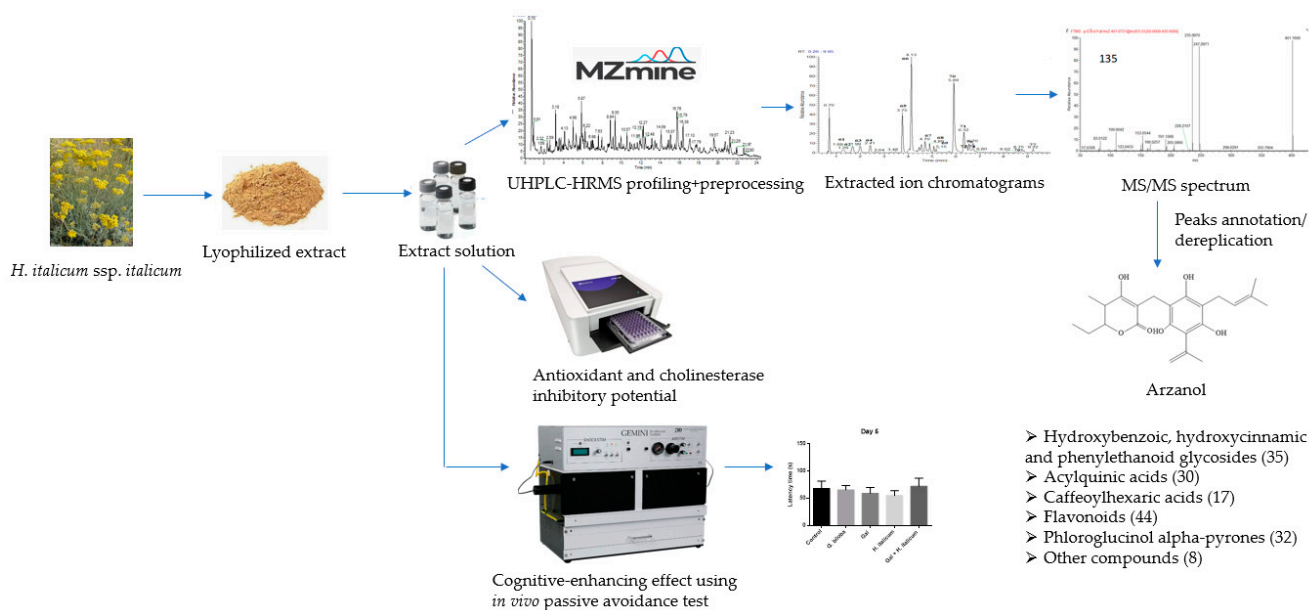
Figure 1. A flow chart for the design of the experiment.

2.1. UHPLC-HRMS Profiling of H. italicum Extract

Herein, a comprehensive UHPLC-HRMS analysis of *H. italicum* methanol–aqueous extract was performed yielding the identification/annotation of more than 160 secondary metabolites (Tables 1 and S1). The total ion chromatogram (TIC) in the negative ion mode of the studied extract was depicted in Figure 2.
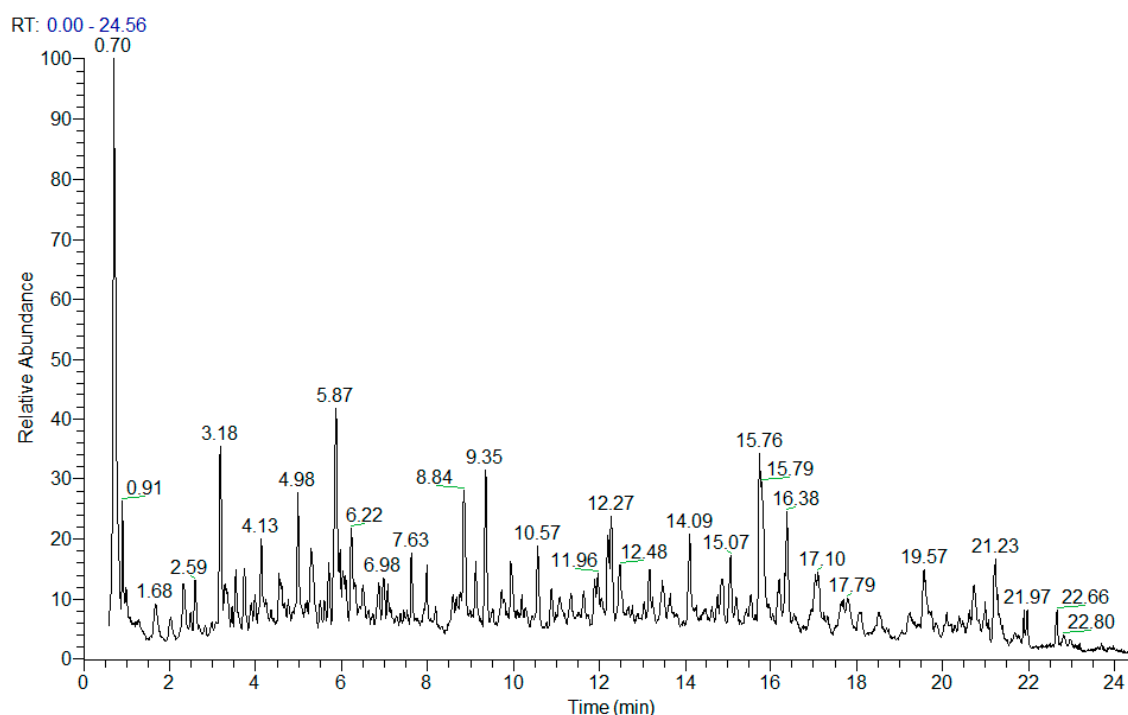
Figure 2. TIC in negative ion mode of *H. italicum* extract.

For the first time, 12 phenolic acids and derivatives and coumarins, 14 acylquinic acids, 15 acylhexaricic acids, 22 flavonoid aglycones and glycosides, and 28 heterodimer-pyrones were reported in *H. italicum* (Table 1, Figures S1–S6). To the best of our knowledge, phenylethanoid glycosides, a series of hydroxybenzoic and hydroxicinnamic acid–glycosides, hydroxycinnamoyl hexoses (sugar esters), caffeoyl-hydroxydihydrocaffeoylquinic, malonyl-dicaffeoylquinic, *p*-coumaroyl-caffeoylquinic and tricaffeoylquinic acids, and di-caffeoylquinic acid-hexoside were reported for the first time. Within a group of acyl-hexaric acids, hydroxybutanyl-tricaffeoylhexaric, isobutanyl-tricaffeoylhexaric, and 2-methyllbutanyl/isovaleryl-tricaffeoylhexaric acids were not previously reported in the literature. A series of methoxylated derivatives of scutellarein, quercetagetin, and 6-hydroxyluteolin together with flavonol-hydroxycinnamoylglycosides represent new secondary metabolites in the species. This study is the first attempt at an in-depth characterization of phloroglucinol α-pyrones by hyphenated technique LC-MS allowing for the annotation of a series of heterodimers not previously reported even in the genus *Helichrysum*. It is worth noting that the fragmentation patterns of four subclasses of pyrones are suggested (Tables S1 and S2, Figures 1 and S7–S11).

2.2. Hydroxybenzoic, Hydroxycinnamic Acids and Their Derivatives

A variety of hydroxybenzoic and hydroxycinnamic acid hexosides was tentatively identified including **1–3**, **6–10**, **16–18**, **20**, **21**, and **23** (Tables 1 and S1).

MS/MS spectra of sugar esters hydroxybensoyl-hexose (**5**), vanillyl-hexose (**11**), and syringoyl-hexose (**13**) were acquired. In contrast to the analogous hexosides, the precursor ions afforded fragment ions resulting from the hexose cross ring cleavages as $^{0.4}$Hex (−60 Da), $^{0.3}$Hex (−90 Da), and $^{0.2}$Hex (−120 Da) [18] (Figure 3).
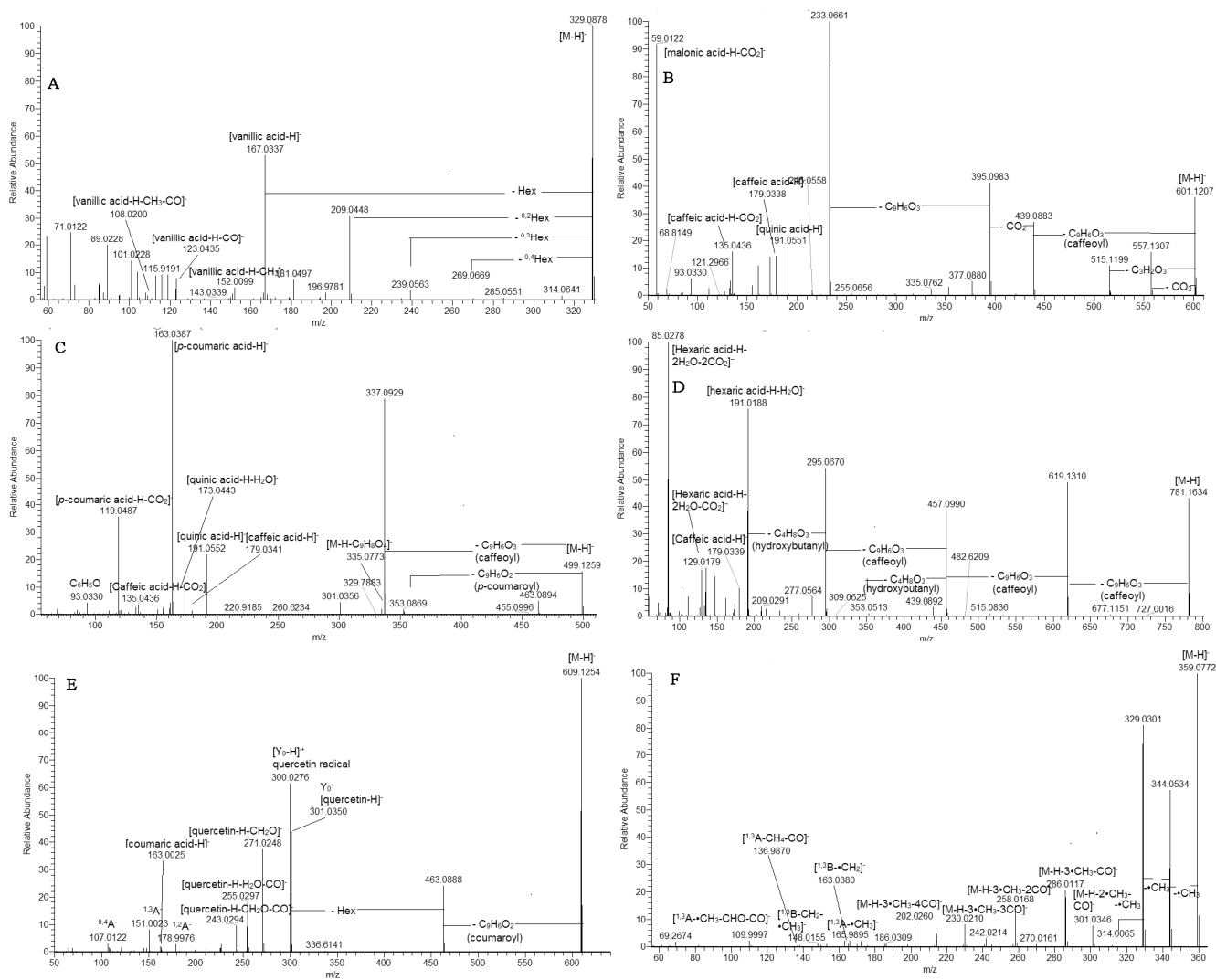
Figure 3. MS/MS spectra of vanillyl O-hexose (**11**) (**A**), 1,3-dicaffeoylquinic acid malonyl (**53**) (**B**), 3-*p*-coumaroyl-5-caffeoylquinic acid (**59**) (**C**), hydroxybutanyl-trcaffeoylhexaric acid (**80**) (**D**), quercetin *O*-coumaroylhexoside (**100**) (**E**), and quercetagetin-3,6,3'(4')-trimethyl ether (**119**) (**F**).

Based on the comparison with the retention times and fragmentation patterns of reference standards, six hydroxybenzoic acids (**4**, **14**, **15**, **29**, **30**, and **34**) and four hydroxycinnamic acids (**22**, **26**, **28**, and **31**) together with quinic acid (**19**) and *p*-hydroxyphenylacetic (**25**) were identified in the extract (Table S1, Figure S1).

Within this group, **26** (caffeic acid) was the main compound in the studied extract, together with **19**, **24**, and **25** (Figure S1). Although hydroxybenzoic and hydroxycinnamic acids were present in their free form, herein, a large number of phenolic acids hexosides were revealed in *H. italicum* for the first time. The extracted ion chromatograms of hydroxybenzoic and hydroxycinnamic acids and derivatives showed that the *H. italicum* profile was dominated by caffeic acid (**26**) (13.95%), protocatechuic acid-*O*-hexoside (**2**) (13.10%), dehydrochorismic acid (**27**) (7.88%), and vanillic acid (**30**) (5.20%) together with 4-hydroxybenzoic acid (**14**) (4.74%) and protocatechuic acid (**4**) (4.44%) (Figure S1).

2.3. Acylquinic Acids (AQA)

Ten mono-, nineteen di-, and one triacylquinic acids (AQAs) were identified or annotated in the *H. italicum* extract (Tables 1 and S1, Figure S2). Fragmentation patterns were consistent with those reported elsewhere [19–21]. Thus, **38**/**41**, **42**/**48**, and **46** were assigned to 5-caffeoyl-, 5-*p*-coumaroyl, and 5-feruloylquinic acid, respectively, as the base peak was observed at *m/z*

191.055, while 3-caffeoyl-(**36**) and 3-feruloylquinic acid (**40**) were evidenced by the abundant ions at m/z 179.034 (65%) and 193.050 (100%), respectively (Table S1).

diAQA consisted of the following subclasses: dicaffeoylquinic acids (*di*CQA) (**44**, **51**, **52**, **54**, and **56**), dicaffeoylquinic acid malonyl (**53**, **55**, **57**, and **58**), feruloyl-caffeoylquinic acids (FCQA) (**60**, **61**, **63**, and **64**), *p*-coumaroyl-caffeoylquinic acids (*p*-CoCQA) (**59** and **62**), and hydroxydihydrocaffeoyl-caffeolylquinic acids (HC-CQA) (**43**, **45**, and **47**) (Table S1).

Compounds **59** and **60** afforded prominent ions at m/z 337.093 (81%) and 367.103 (100%), respectively, indicating a loss of caffeoyl residue before the *p*-coumaroyl (**59**) and feruloyl (**60**) moiety. Furthermore, both compounds yielded fragment ions at m/z 163.039 (100%) and 193.050 (93%), respectively, as was observed in 3-AQA together with m/z 119.049 [*p*-coumaric acid-H-CO$_2$]$^-$ (36%) (**59**) and 134.036 [ferulic acid-H-CH$_3$-CO$_2$]$^-$ (63%) (**60**) (Table S1, Figure 3). Thus, **59** and **60** were ascribed as 3-*p*-Co-5CQA and 3F-5CQA, respectively.

Based on the distinctive "dehydrated" peak at m/z 173.045 [quinic acid-H-H$_2$O]$^-$, **62** and **63** were annotated as vicinal 4-*p*-Co-5CQA and 4F-5CQA. Likewise, the vicinal *di*CQA 3, 4-diCQA (**51**), and 4,5-diCQA (**56**) were also defined (Table S1). The assignment of *di*CQA malonyl esters (**53**, **55**, **57**, and **58**) was suggested by the transitions resulting from the loss of 86.001 Da (C$_3$H$_2$O$_3$) or the malonyl group. Thus, **53** produced 601.121→515.120 together with the base peak at m/z 233.066, indicating concomitant loss of two caffeoyl moieties and CO$_2$ (Table S1, Figure 3). Peak **50** afforded a precursor ion at m/z 677.173 (calc. for C$_{31}$H$_{33}$O$_{17}$) together with the transitions at m/z 677.173→515.141→353.088→191.055 resulting from the losses of two caffeoyl residues and hexose unit, respectively (Table S1). The 1,3-*di*substituted quinic acid skeleton was discernible by the ions at m/z 191.055 (82%), 179. 034 (99%), and 135.044 (100%). Thus, **50** was ascribed as 1,3-*di*caffeoylquinic acid-hexoside.

The most lipophilic AQA was **65**; 3,4,5-triCQA was discernable by the prominent ions at m/z 179.034, 173.045, and 135.044, as was observed in the 3,4-disubstituted quinic acid skeleton. Among acylquinic acids, the predominant compounds in *H. italicum* extract were 3,4-dicaffeoylquinic acid (**51**) (18.99%) and 3,5-dicaffeoylquinic acid (**52**) (18.92%), followed by 1,5-dicaffeoylquinic acid (**54**) (15.51%) and 4,5-dicaffeoylquinic acid (**56**) (8.80%) (Figure S2).

2.4. Caffeoylhexaric Acids

Key points in the acylhexaric acids annotation were the subsequent losses of one (**66**–**69**), two (**70**–**74**), and three (**75**–**78**) caffeoyl residues (Tables 1 and S1, Figure S3). Thus, the base peak in the MS/MS spectra was consistent with [hexaric acid (HA)-H]$^-$ at m/z 209.030 (C$_6$H$_9$O$_8$) supported by the series of prominent ions at m/z 191.019 [HA-H-H$_2$O]$^-$, 147.029 [HA-H-H$_2$O-CO$_2$]$^-$, 129.018 [HA-H-2H$_2$O-CO$_2$]$^-$, 111.007 [HA-H-3H$_2$O-CO$_2$]$^-$, and 85.028 [HA-H-2H$_2$O-2CO$_2$]$^-$ (Table S1) [22]. Compounds **79** and **80** shared the same [M-H]$^-$ at m/z 781.162 (calc. for C$_{37}$H$_{34}$O$_{19}$ (Table S1, Figure 3). They produced the indicative fragment ions at m/z 353.052 [M-H-2caffeoyl-C$_4$H$_8$O$_3$]$^-$ and 191.019 [M-H-3caffeoyl-C$_4$H$_8$O$_3$]$^-$ resulting from the concomitant losses of caffeoyl residues and hydroxybutyric acid. Caffeoyl moiety was suggested by the fragment ions at m/z 179.0.4 [caffeic acid (CA)-H]$^-$, 161.023 [(CA-H)-H$_2$O]$^-$, and 135.044 [(CA-H)-CO$_2$]$^-$. Compounds **79** and **80** were ascribed as isomeric hydroxybutanyl-tricaffeoylhexaric acids. Similarly, **81** ([M-H]$^-$ at m/z 765.167, C$_{37}$H$_{34}$O$_{18}$) was assigned to isobutanyl-tricaffeoylhexaric acids as indicated by the transition 279.072→191.019, suggesting a loss of 88.054 Da (calc. for C$_4$H$_8$O$_2$) or isobutyric acid. In the same manner, 2-methylbutanyl/isovaleryl residue in **82** was deduced from the prominent ions at 293.088 [M-H-3caffeoyl]$^-$ and a subsequent loss of 102.069 Da (calc. for C$_5$H$_{10}$O$_2$) or 2-methylbutiric acid/isovaleric acid at m/z 191.019 (Table S1). Thus, **82** was ascribed as 2-methylbutanyl/isovaleryl-tricaffeoylhexaric acid.

Among caffeoylhexaric acids, tricaffeoylhexaric acid 1 (**75**) (22.01%), together with its isomers **76** (11.93%), **77** (11.11%), and **78** (10.92%), appeared to be dominant for *H. italicum* extract (Figure S3).

2.5. Flavonoids

Typical ions of the *O*-glycosyl flavonoid pathway were produced in a variety of flavones and flavonol-hexosides including **83**, **85–87**, **89–91**, **94**, **96**, and **97** (Tables 1 and S1, Figure S4).

In (-) ESI mode, the precursor ions provided the relevant ions at m/z 317.030 (myricetin), 301.035/300.028 (quercetin), 285.040 (luteolin and kaempferol), 331.046 (patuletin), 329.066 (jaceosidin), 315.047 (nepetin and isorhamnetin), and 299.056 (hispidulin). A 6-methoxylated flavonoid skeleton was discernable by the RDA ions at m/z 165.990 ($^{1,3}A^-$—CH_3), 164.982 ($^{1,3}A^-$—CH_4), 163.002 ($^{1,3}A^-$—H_2O), and 136.987 ($^{1,3}A^-$-CH_4-CO) [13,14]. In addition, a low abundant ion at 181.013 ($^{1,3}A^-$) was registered in the fragmentation pattern of patuletin and 6-methoxykaempferol.

The two compounds **88** and **92** shared the same [M-H]$^-$ at m/z 505.099, yielding prominent fragment ions at m/z 463.086.094 [M-H-C_2H_2O]$^-$ (**88**) and m/z 301.035 [M-H-(C_2H_2O+Hex)]$^-$, indicating a subsequent loss of an acetyl group (42 Da) and hexosyl (162 Da) (Table S1). In addition to the aglycone quercetin (Y_0^-), an abundant radical aglycone [Y_0-H]$^{-\bullet}$ was also formed, suggesting a 3-*O*-glycosidic bond [23]. In the same manner, kaempferol 3-*O*- and myricetin 3-*O*-acetylhexoside were depicted in flavonoid profiling.

The two compounds **109** ([M-H]$^-$ at m/z 609.125) and **111** ([M-H]$^-$ at m/z 639.136) shared the same fragmentation patterns yielding prominent fragment ions at m/z 447.092 (**109**) and 477.104 (**111**), respectively, resulting from loss of a caffeoyl moiety (162 Da, $C_9H_6O_3$) (Table S1). Moreover, caffeoyl moiety was evidenced by the fragment ions at m/z 179.034 [(caffeic acid-H)]$^-$ (**109**), 161.023 [(caffeic acid-H)-H_2O]$^-$, and 135.044 [(caffeic acid-H)-CO_2]$^-$. Consequently, **109** was ascribed as kempferol *O*-caffeoylhexoside, while **111** was annotated as isorhamnetin *O*-caffeoylhexoside.

In the same way, **98/100**, **103/108**, and **107/110** were assigned to coumaroyl esters of quercetin-, kaempferol, and isorhamnetin *O*-hexoside (Table S1, Figure S4). The commonly found losses of 146 Da ($C_9H_6O_2$) and 308 Da ($C_{15}H_{16}O_7$) in the fragmentation patterns of the aforementioned compounds accompanied with the ions at m/z 163.039 [coumaric acid-H]$^-$ and 145.028 [(coumaric acid-H)-H_2O]$^-$ confirmed the presence of a coumaroyl moiety. One feruloyl ester of quercetin-hexoside (**99**) was evidenced on the base of the loss of 176 Da ($C_{10}H_8O_3$) at m/z 463.088 023 and 338 Da ($C_{16}H_{18}O_8$) at m/z 301.0349 (Table S1, Figure 3). A malonyl ester **93** was discernable by the transition [M-H]$^-$→Y_0 resulting from the indicative loss of 248.046 Da ($C_9H_{12}O_8$).

The approach for 6-methoxylated flavonoids annotation was delineated elsewhere [12–14]. Among them, five methoxylated derivatives of quercetagetin (**112**, **119**, and **122**), scutelarein (**113**), and 6-hydroxyluteolin (**117**) were described (Table S1, Figure S5).

As an example, compound **119** ([M-H]$^-$ at m/z 359.077, $C_{18}H_{15}O_8$) was used to illustrate the fragmentation pattern of 6-methoxylated quercetagetin derivatives (Table S1). In (-) ESI-MS/MS, **119** afforded typical radical losses at m/z 344.054 [M-H-•CH_3]$^-$, 329.030 [M-H-2•CH_3]$^-$, and 314.007 [M-H-3•CH_3]$^-$, accompanied with subsequent neutral losses at m/z 301.035 [M-H-2•CH_3-CO]$^-$, 286.012 [M-H-3•CH_3-CO]$^-$, 258.017 [M-H-3•CH_3-2CO]$^-$, 230.021 [M-H-3•CH_3-3CO]$^-$, and 202.026 [M-H-3•CH_3-4CO]$^-$ (Figure 3). The precursor ion yielded a series of low abundant fragment RDA ions at m/z 165.990 ($^{1,3}A^-$-•CH_3), 136.987 ($^{1,3}A^-$-CO-CH_4), and 109.9997 ($^{1,3}A^-$-CO-CHO-CH_3), indicating methoxylation in the A-ring (Ren et al., 2018). On the other hand, prominent fragment ions at m/z 163.038 ($^{1,3}B^-$-CH_2) and $^{1,3}B^-$ at m/z 148.016 ($^{1,3}B^-$-•CH_3-CH_2) (Table S1) pointed out a dimethoxylated RDA ion $^{1,3}B$. Thus, **119** and **122** were ascribed as quercetagetin-3,6,3'(4')-trimethyl ether. In line with Kramberger et al. [7], either initial RDA ions or their derivatives were not registered in **118** (gnaphaliin) with m/z [M-H]$^-$ at m/z 313.072, $C_{17}H_{13}O_6$ (Table S1). In addition to the abundant ions at m/z 298.048 and 283.025 resulting from the radical losses, a series of neutral losses (CO and CO_2) was also generated at m/z 199.039 [M-H-2•CH_3-3CO]$^-$, 183.044 [M-H-2•CH_3-2CO-CO_2]$^-$, and 139.054 [M-H-2•CH_3-2CO-2CO_2]$^-$.

In the MS/MS spectra of pinocembrin (**123**) and galangin (**124**), the corresponding $^{1,3}B$ ions were not found—both compounds have no substitution on the B-ring.

Overall, galangin methyl ether (**126**) (18.43%) and gnaphaliin 2 (**125**) (14.71%) were found to be the predominant flavonoids followed by hyperoside (**85**) (7.44%), quercetin 7,3′(4′)-dimethyl ether (**120**) (4.80%), quercetin *O*-coumaroylhexoside isomer (**98**) (4.68%), and quercetin *O*-coumaroylhexoside 2 (**100**) (4.67) (Figures S4 and S5).

2.6. Prenylated Phloroglucinol α-Pyrones

Pyrones refer to the special class heterodimers consisting of prenylated phloroglucinyl and α-pyrone [24]. In the MS/MS spectra, all the [M-H]⁻ lose α-pyrone moieties and form abundant peaks [M-H-pyrone]⁻ (Tables 1 and S1, Figures S6–S11). Hence, the characteristic neutral losses of *m/z* 140.048 ($C_7H_8O_3$), 154.063 ($C_8H_{10}O_3$), 168.079 ($C_9H_{12}O_3$), 182.095 ($C_{10}H_{14}O_3$) Da was employed to recover α-pyrone residue in each derivative. Pyrones typically cleave at C-7 and accordingly lose additional carbon (−12 Da) as follows: *m/z* 152.048 ($C_8H_8O_3$), 166.063 ($C_9H_{10}O_3$), 180.079 ($C_{10}H_{12}O_3$), and 194.095 Da ($C_{11}H_{14}O_3$) (Table S1). Diagnostic fragment ions for the corresponding pyrone units were registered in the (-) ESI-MS/MS spectra at *m/z* 139.039 ($C_7H_7O_3$), 153.054 ($C_8H_9O_3$), 167.070 ($C_9H_{11}O_3$), and 181.086 ($C_{10}H_{13}O_3$). In addition, all pyrone units provided [Pyrone-H-CO$_2$]⁻ at *m/z* 95.048, 109.064, 123.080, and 137.096, respectively. Accordingly, in the (+) ESI-MS/MS spectra, fragment ions at *m/z* 141.055 ($C_7H_9O_3$), 155.070 ($C_8H_{11}O_3$), 169.086 ($C_9H_{13}O_3$), and 183.102 ($C_{10}H_{15}O_3$) were produced.

Thus, a methyl group at C-11 in the α-pyrone unit was deduced in arenol (**131**) and **148**. The majority of the pyrones were assigned to phloroglucinyl α-pyrones possessing an ethyl group at C-11. An isopropyl group was evidenced at C-11 of **130**, **139**, **144**, and **157**, while 1-methyl-propyl moiety was found in **143**, **149**, and **150**. Accordingly, four subclasses of pyrones were suggested as follows: methylpyrones (MP), ethylpyrones (EP), isopropylpyrones (IPP), and 1-methyl-propylpyrones (MPP). The tentative structures of phloroglucinyl α-pyrones are depicted in Table S2.

Exemplified by **135** ([M-H]⁻ at 401.160), in (-) ESI-MS, phloroglucinol skeleton gave prominent fragment ions at *m/z* 205.086 [M-H-$C_8H_{10}O_3$-C_2H_2O]⁻, 191.107 [M-H-$C_8H_{10}O_3$-2CO]⁻, and 166.026 [M-H-$C_9H_{10}O_3$-C_5H_9]⁻, indicating a loss of an acyl group at C-1 and a prenyl chain at C-3, respectively (Figures 4 and S8). On the other hand, in (+) ESI-MS/MS, the base peak at *m/z* 181.050 resulted from the typical concomitant losses of (α-pyrone-C, $C_9H_{10}O_3$) and C_4H_8. Thus, **135** was assigned as arzanol [25,26]. An MS/MS spectrum of **141** was acquired. [M-H]⁻ at *m/z* 415.175 (calc. for $C_{23}H_{27}O_7$) indicated 14 Da higher than that of **135**, suggesting an additional methylene group and an oxopropyl moiety at C-1. This assumption was confirmed by the indicative fragment ions in (+) ESI-MS at *m/z* 417.190 [M+H-C_4H_8]⁺ and 195.065 [M+H-$C_9H_{10}O_3$-C_4H_8]⁺. In the same manner, in (+) ESI-MS, **146** gave [M+H]⁺ at *m/z* 431.206 (calc. for $C_{24}H_{31}O_7$) and prominent fragment ions at *m/z* 375.143 [M+H-C_4H_8]⁺ and 209.081 [M+H-$C_9H_{10}O_3$-C_4H_8]⁺ consistent with a prenyl group at C-3 and 2-methyl-oxopropyl residue at C-1 as was seen in 6-*O*-desmethyllauricepyrone isolated from *H. oocephalum* and *H. stenopterum* DC (Figures S8 and S11) [24]. Compound **151** yielded [M-H]⁻ at *m/z* 443.208 ($C_{25}H_{31}O_7$), indicating an additional methylene group compared to **146**. Ethylpyrone moiety was evidenced by the typical neutral losses at *m/z* 291.159 [M+H-$C_8H_{10}O_3$]⁺ and 279.159 [M+H-$C_9H_{10}O_3$]⁺ accompanied by the subsequent loss of 56 Da (C_4H_8) at *m/z* 235.096 and 223.0963, respectively (Table S1). Thus, 2-methyl-oxobutyl residue was dedicated at C-1, and **151** could be ascribed as 23-methyl-6-*O*-desmethyllauricepyrone isolated previously from *H. stenopterum* and *H. oocephalum* [24,27]. The abovementioned functional groups at C-1 of phloroglucinol moiety were consistent with those evidenced in the heterodimeric pyrones from *H. italicum* subsp. *microphyllum* [6] and the prenylated phloroglucinols isolated from *H. paronichioides* [28].
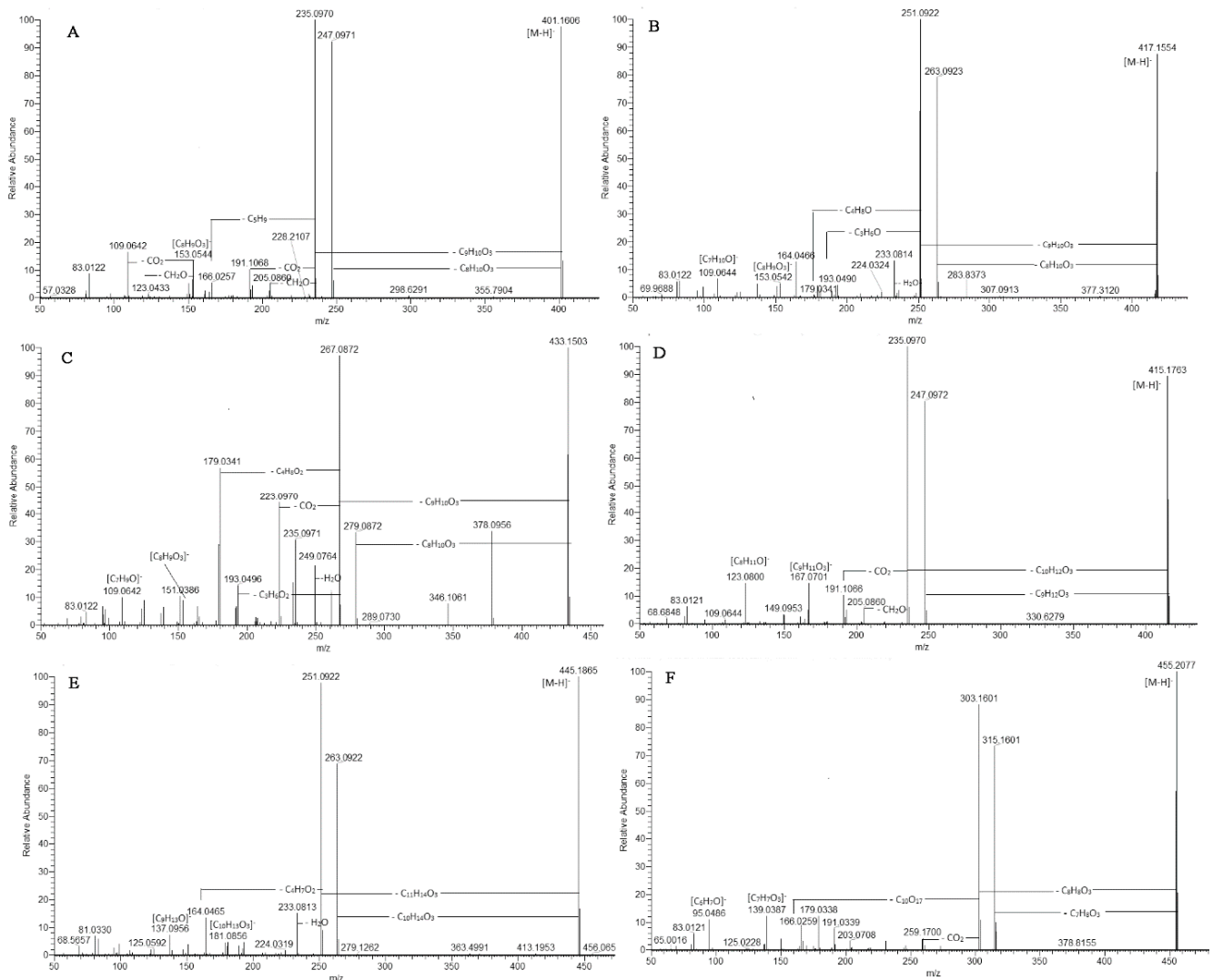
Figure 4. MS/MS spectra of phloroglucinol alpha-pyrones; compounds **135** (**A**), **140** (**B**), **128** (**C**), **139** (**D**), **149** (**E**), and **148** (**F**).

Table 1. Secondary metabolites in *Helichrysum italicum* methanol–aqueous extract.

№	Identified/Tentatively Annotated Compound	Molecular Formula	Exact Mass [M-H]$^-$	t_R (min)	Δ ppm	Level of Confidence [21,29]	References
	Hydroxybenzoic, hydroxycinnamic, and phenylethanoid glycosides						
1.	hydroxybenzoic acid-*O*-hexoside	$C_{13}H_{16}O_8$	299.0778	1.28	−3.279	2	[9]
2.	protocatechuic acid-*O*-hexoside	$C_{13}H_{16}O_9$	315.0727	1.68	0.115	2	[9]
3.	vanillic acid-*O*-hexoside	$C_{14}H_{18}O_9$	329.0875	1.75	−0.198	2	[9]
4.	protocatechuic acid [a]	$C_7H_6O_4$	153.0181	2.02	−1.392	1	[26]
5.	hydroxybenzoyl hexose [b]	$C_{13}H_{16}O_8$	299.0778	2.04	0.002	2	
6.	protocatechuic acid-*O*-hexoside isomer	$C_{13}H_{16}O_9$	315.0727	2.11	1.729	2	

Table 1. *Cont.*

№	Identified/Tentatively Annotated Compound	Molecular Formula	Exact Mass [M-H]$^-$	t_R (min)	Δ ppm	Level of Confidence [21,29]	References
7.	*p*-hydroxyphenylacetic acid *O*-hexoside [b]	$C_{14}H_{18}O_8$	313.0932	2.12	0.988	2	
8.	syringic acid-*O*-hexoside [b]	$C_{15}H_{20}O_{10}$	359.0985	2.24	0.036	2	
9.	caffeic acid-*O*-hexoside	$C_{15}H_{18}O_9$	341.0871	2.41	−1.980	2	
10.	hydroxybenzoic acid-*O*-hexoside isomer	$C_{13}H_{16}O_8$	299.0778	2.44	0.800	2	
11.	vanillyl *O*-hexose [b]	$C_{14}H_{18}O_9$	329.0875	2.47	0.075	2	
12.	esculetin-*O*-hexoside [b]	$C_{15}H_{15}O_9$	339.0724	2.70	0.515	2	
13.	syringyl-*O*-hexose [b]	$C_{15}H_{20}O_{10}$	359.0984	2.75	−0.278	2	
14.	4-hydroxybenzoic acid [a]	$C_7H_6O_3$	137.0230	2.83	−10.928	2	[26] [9]
15.	gentisic acid [a]	$C_7H_6O_4$	153.0181	2.98	−8.051	1	
16.	*p*-hydroxyphenylacetic acid *O*-hexoside isomer [b]	$C_{14}H_{18}O_8$	313.0929	2.99	0.030	2	
17.	hydroxybenzoic acid-*O*-hexoside	$C_{13}H_{16}O_8$	299.0778	2.99	−0.704	2	[9]
18.	caffeic acid *O*-hexoside	$C_{15}H_{18}O_9$	341.0871	3.07	−0.602	2	
19.	quinic acid	$C_7H_{12}O_6$	191.0549	3.18	−5.817	2	[26]
20.	caffeic acid-*O*-hexoside	$C_{15}H_{18}O_9$	341.0871	3.27	−0.386	2	[9]
21.	coumaric acid-*O*-hexoside	$C_{15}H_{18}O_8$	325.0930	3.34	−3.355	2	[26] [9]
22.	*p*-coumaric acid [a]	$C_9H_8O_3$	163.0389	3.35	−8.203	1	[26]
23.	vanillic acid *O*-hexoside isomer	$C_{14}H_{18}O_9$	329.0875	3.37	0.252	2	[9]
24.	esculetin	$C_9H_6O_4$	177.0193	3.46	4.982	2	[9]
25.	*p*-hydroxyphenylacetic acid [a,b]	$C_8H_8O_3$	151.0401	3.46	−9.252	2	
26.	caffeic acid [a]	$C_9H_8O_4$	179.0339	3.54	−6.044	1	[26]
27.	dehydrochorismic acid [b]	$C_{10}H_8O_6$	223.0248	3.73	−7.180	2	
28.	*m*-coumaric acid [a,b]	$C_9H_8O_3$	163.0389	4.56	−7.958	1	
29.	syringic acid [a]	$C_9H_{10}O_5$	197.0446	4.76	−4.703	1	[26]
30.	vanillic acid [a,b]	$C_8H_8O_4$	167.0338	4.78	−7.615	1	
31.	*o*-coumaric acid [a,b]	$C_9H_8O_3$	163.0389	5.01	−7.958	1	
32.	scopoletin	$C_{10}H_8O_4$	191.0350	5.06	−5.088	2	[6]
33.	caffeic acid *O*-(hydroxyisovaleryl)-hexoside [b]	$C_{20}H_{26}O_{11}$	441.1402	5.58	0.125	2	
34.	salicylic acid [a]	$C_7H_6O_3$	137.0230	6.27	−10.344	1	26]
35.	caffeic acid *O*-(hydroxybensoyl)-hexoside [b]	$C_{22}H_{22}O_{11}$	461.1089	8.26	0.142	1	

			Mono-, di-, and triacylquinic acids				
36.	neochlorogenic (3-caffeoylquinic) acid [a,b]	$C_{16}H_{18}O_9$	353.0867	2.35	0.495	1	
37.	3-*p*-coumaroylquinic acid	$C_{16}H_{18}O_8$	337.0928	3.02	1.096	2	
38.	chlorogenic (5-caffeoylquinic) acid [a]	$C_{16}H_{18}O_9$	353.0874	3.18	0.665	1	[9,26]
39.	4-caffeoylquinic acid	$C_{16}H_{18}O_9$	353.0878	3.35	−0.100	2	[9]
40.	3-feruloylquinic acid	$C_{17}H_{20}O_9$	367.1034	3.43	−0.096	2	[26]
41.	5-caffeoylquinic acid isomer	$C_{16}H_{18}O_9$	353.0874	3.88	0.580	2	[9]
42.	5-*p*-coumaroylquinic acid	$C_{16}H_{18}O_8$	337.0928	3.96	0.829	2	[9]

Table 1. *Cont.*

№	Identified/Tentatively Annotated Compound	Molecular Formula	Exact Mass [M-H]$^-$	t_R (min)	Δ ppm	Level of Confidence [21,29]	References
43.	3-caffeoyl-5-hydroxy-dihydrocaffeoylquinic acid [b]	$C_{25}H_{26}O_{13}$	533.1288	4.03	0.236	2	
44.	1, 3- dicaffeoylquinic acid [b]	$C_{25}H_{24}O_{12}$	515.1190	4.14	0.137	2	
45.	3-caffeoyl-4- hydroxy-dihydrocaffeoylquinic acid [b]	$C_{25}H_{26}O_{13}$	533.1288	4.37	2.1	2	
46.	5-feruloylquinic acid	$C_{17}H_{20}O_9$	367.1034	4.42	−0.096	2	[9]
47.	1-caffeoyl-3-hydroxy-dihydrocaffeoylquinic acid [b]	$C_{25}H_{26}O_{13}$	533.1288	4.45	12.710	2	
48.	5-*p*-coumaroylquinic acid isomer	$C_{16}H_{18}O_8$	337.0928	4.63	0.028	2	[9]
49.	4-feruloylquinic acid [b]	$C_{17}H_{20}O_9$	367.1034	4.69	−0.260	2	
50.	1,3-dicaffeoylquinic acid-hexoside	$C_{31}H_{34}O_{17}$	677.1723	5.15	0.956	2	[9]
51.	3,4-dicaffeoylquinic acid [a]	$C_{25}H_{24}O_{12}$	515.1190	5.71	0.254	1	[9,26]
52.	3,5-dicaffeoylquinic acid [a]	$C_{25}H_{24}O_{12}$	515.1189	5.85	0.370	1	[9]
53.	1,3-dicaffeoylquinic acid malonyl [b]	$C_{28}H_{26}O_{15}$	601.1199	5.95	1.292	2	
54.	1,5-dicaffeoylquinic acid [a]	$C_{25}H_{24}O_{12}$	515.1190	6.03	−0.096	1	[9]
55.	3, 5-dicaffeoylquinic acid malonyl [b]	$C_{28}H_{26}O_{15}$	601.1199	6.15	−0.039	2	
56.	4,5-dicaffeoylquinic acid	$C_{25}H_{24}O_{12}$	515.1190	6.24	0.254	2	[9]
57.	3, 4-dicaffeoylquinic acid malonyl [b]	$C_{28}H_{26}O_{15}$	601.1199	6.32	0.577	2	
58.	4, 5-dicaffeoylquinic acid malonyl [b]	$C_{28}H_{26}O_{15}$	601.1199	6.51	0.677	2	
59.	3-*p*-coumaroyl-5-caffeoylquinic acid [b]	$C_{25}H_{24}O_{11}$	499.1251	6.53	2.535	2	
60.	3-feruloyl-5-caffeoylquinic acid	$C_{26}H_{26}O_{12}$	529.1356	6.83	−0.849	2	[9]
61.	3-caffeoyl-5-feruloylquinic acid [b]	$C_{26}H_{26}O_{12}$	529.1356	6.90	0.776	2	
62.	4-*p*-coumaroyl-5-caffeoylquinic acid [b]	$C_{25}H_{24}O_{11}$	499.1252	6.94	−4.117	2	
63.	4-feruloyl-5-caffeoylquinic acid	$C_{26}H_{26}O_{12}$	529.1356	7.09	−0.037	2	[9]
64.	4-caffeoyl-5-feruloylquinic acid [b]	$C_{26}H_{26}O_{12}$	529.1356	7.18	0.474	2	
65.	3,4,5-tricaffeoylquinic acid [a]	$C_{34}H_{30}O_{15}$	677.1528	7.78	1.605	1	
			Caffeoylhexaric acids				
66.	caffeoylhexaric acid [b] 1	$C_{15}H_{16}O_{11}$	371.0620	1.29	1.470	2	
67.	caffeoylhexaric acid [b] 2	$C_{15}H_{16}O_{11}$	371.0620	1.69	−1.979	2	
68.	caffeoylhexaric acid [b] 3	$C_{15}H_{16}O_{11}$	371.0620	1.99	−4.028	2	
69.	caffeoylhexaric acid [b] 4	$C_{15}H_{16}O_{11}$	371.0620	2.41	−6.956	2	
70.	dicaffeoylhexaric acid 1	$C_{24}H_{22}O_{14}$	533.0937	3.75	0.134	2	[9]
71.	dicaffeoylhexaric acid [b] 2	$C_{24}H_{22}O_{14}$	533.0937	4.13	−8.213	2	
72.	dicaffeoylhexaric acid [b] 3	$C_{24}H_{22}O_{14}$	533.0937	4.71	−14.066	2	
73.	dicaffeoylhexaric acid [b] 4	$C_{24}H_{22}O_{14}$	533.0937	4.89	−14.516	2	

Table 1. *Cont.*

№	Identified/Tentatively Annotated Compound	Molecular Formula	Exact Mass [M-H]$^-$	t_R (min)	Δ ppm	Level of Confidence [21,29]	References
74.	dicaffeoylhexaric acid [b] 5	$C_{24}H_{22}O_{14}$	533.0937	5.15	−8.457	2	
75.	tricaffeoylhexaric acid 1	$C_{33}H_{28}O_{17}$	695.1254	5.89	0.788	2	[9]
76.	tricaffeoylhexaric acid [b] 2	$C_{33}H_{28}O_{17}$	695.1254	6.32	1.219	2	
77.	tricaffeoylhexaric acid [b] 3	$C_{33}H_{28}O_{17}$	695.1254	6.44	1.133	2	
78.	tricaffeoylhexaric acid [b] 4	$C_{33}H_{28}O_{17}$	695.1254	6.53	2.011	2	
79.	hydroxybutanyl-trcaffeoylhexaric acid [b] 1	$C_{37}H_{34}O_{19}$	781.1622	6.53	0.177	2	
80.	hydroxybutanyl-trcaffeoylhexaric acid [b] 2	$C_{37}H_{34}O_{19}$	781.1622	6.66	1.585	2	
81.	isobutanyl-tricaffeoylhexaric acid [b]	$C_{37}H_{34}O_{18}$	765.1672	8.54	1.755	2	
82.	2-methyllbutanyl/isovaleryl-tricaffeoylhexaric acid [b]	$C_{38}H_{36}O_{18}$	779.1829	9.21	1.531	2	
		Flavonoids					
83.	myricetin *O*-hexoside	$C_{21}H_{20}O_{13}$	479.0831	4.55	0.159	2	[9,26]
84.	myricetin *O*-acetylhexoside	$C_{23}H_{22}O_{14}$	521.0939	5.19	0.483	2	[9]
85.	hyperoside [a]	$C_{21}H_{20}O_{12}$	463.0885	5.29	0.520	1	[9,26]
86.	luteolin-7-*O*-glucoside [a,b]	$C_{21}H_{20}O_{11}$	447.0934	5.31	0.213	1	
87.	patuletin *O*-hexoside [b]	$C_{22}H_{22}O_{13}$	493.0987	5.50	0.783	2	
88.	quercetin *O*-acetylhexoside [b] 1	$C_{23}H_{22}O_{13}$	505.0988	5.61	0.666	2	
89.	nepetin *O*-hexoside [b]	$C_{22}H_{22}O_{12}$	447.1038	5.68	−0.061	2	
90.	kaempferol 3-*O*-glucoside [a]	$C_{21}H_{20}O_{11}$	447.0934	5.88	0.258	1	[9,26]
91.	isorhamnetin 3-*O*-glucoside [a]	$C_{22}H_{22}O_{12}$	477.1038	6.03	−0.124	1	[9,26]
92.	quercetin *O*-acetylhexoside isomer [b] 2	$C_{23}H_{22}O_{13}$	505.0988	6.06	−0.859	2	
93.	quercetin *O*-malonylhexoside	$C_{24}H_{22}O_{15}$	549.0886	6.06	−4.722	2	[9]
94.	6-methoxykaempferol *O*-hexoside [b]	$C_{22}H_{22}O_{12}$	477.1038	6.25	−1.340	2	
95.	kaempferol *O*-acetylhexoside	$C_{23}H_{22}O_{12}$	489.1038	6.28	0.308	2	[9]
96.	hispidulin *O*-hexoside [b]	$C_{22}H_{22}O_{11}$	461.1089	6.32	0.792	2	
97.	jaceosidine *O*-hexoside [b]	$C_{23}H_{24}O_{12}$	491.1195	6.50	1.875	2	
98.	quercetin *O*-coumaroylhexoside isomer	$C_{30}H_{26}O_{14}$	609.1250	7.07	0.643	2	[9,26]
99.	quercetin *O*-feruloylhexoside [b]	$C_{31}H_{28}O_{15}$	639.1355	7.20	0.308	2	
100.	quercetin *O*-coumaroylhexoside 2	$C_{30}H_{26}O_{14}$	609.1250	7.30	0.643	2	[9,26]
101.	luteolin [a,b]	$C_{15}H_9O_7$	285.0406	7.58	−0.952	1	
102.	quercetin [a]	$C_{15}H_{10}O_7$	301.0354	7.62	−0.252	1	[26]
103.	kaempferol *O*-coumaroylhexoside 1	$C_{30}H_{26}O_{13}$	593.1301	7.69	1.039	2	[9,26]
104.	patuletin [b]	$C_{16}H_{12}O_8$	331.0464	7.72	−0.304	2	
105.	herbacetin methyl ether	$C_{16}H_{12}O_7$	315.0510	7.76	0.679	2	[9]

Table 1. *Cont.*

№	Identified/Tentatively Annotated Compound	Molecular Formula	Exact Mass [M-H]⁻	t_R (min)	Δ ppm	Level of Confidence [21,29]	References
106.	nepetin [b]	$C_{16}H_{12}O_7$	315.0510	7.76	0.679	2	
107.	isorhamnetin *O-p*-coumaroylhexoside isomer [b] 1	$C_{31}H_{28}O_{14}$	623.1406	7.88	0.981	2	
108.	kaempferol *O*-coumaroylhexoside isomer 2	$C_{30}H_{26}O_{13}$	593.1301	7.95	1.072	2	[9,26]
109.	kaempferol *O*-caffeoylhexoside [b]	$C_{30}H_{26}O_{14}$	609.1250	7.99	0.364	2	
110.	isorhamnetin *O-p*-coumaroylhexoside isomer [b] 2	$C_{31}H_{28}O_{14}$	623.1406	8.08	1.174	2	
111.	isorhamnetin *O*-caffeoylhexoside [b]	$C_{31}H_{28}O_{15}$	639.1355	8.12	0.496	2	
112.	axillarin [b] (quercetagetin 3,6-dimethylether)	$C_{17}H_{14}O_8$	345.0616	8.19	0.027	2	
113.	hispidulin [b]	$C_{16}H_{12}O_6$	299.0561	8.84	0.430	2	
114.	kaempferol [a]	$C_{15}H_9O_7$	285.0406	8.84	−0.531	1	[26]
115.	naringenin	$C_{15}H_{12}O_5$	271.0612	8.86	0.468	1	[9]
116.	isorhamnetin [a]	$C_{16}H_{12}O_7$	315.0510	9.12	0.013	1	[9,26]
117.	jaceosidin [b] (6-hydroxyluteolin-6,3′-dimethyl ether) [a,b]	$C_{17}H_{14}O_7$	329.0677	9.40	0.286	1	
118.	gnaphaliin 1	$C_{17}H_{14}O_6$	313.0718	9.52	0.443	2	[9,26]
119.	quercetagetin-3,6,3′(4′)-trimethyl ether [b] 1	$C_{18}H_{16}O_8$	359.0772	9.66	0.444	2	
120.	quercetin 7,3′(4′)-dimethyl ether [b]	$C_{17}H_{13}O_7$	329.0667	9.71	0.073	2	
121.	kaempferid/isokampferid	$C_{16}H_{12}O_6$	299.0561	9.99	−0.561	2	[9]
122.	quercetagetin-3,6,3′(4′)-trimethyl ether [b] 2	$C_{18}H_{16}O_8$	359.0772	11.18	−0.002	2	
123.	pinocembrin	$C_{15}H_{12}O_4$	255.0663	11.63	−1.302	2	[9,26]
124.	galangin	$C_{15}H_{10}O_5$	269.0457	11.74	−0.954	2	[26]
125.	gnaphaliin 2	$C_{17}H_{14}O_6$	313.0718	12.19	0.123	2	[9,26]
126.	galangin methyl ether	$C_{16}H_{12}O_5$	283.0612	12.27	−0.342	2	[9]

	Pyrones (phloroglucinol alpha-pyrones)						
№	Subclass (tentatively identified compound)	Molecular formula	Exact mass [M-H]⁻	t_R (min)	Δ ppm	Level of confidence	References
127.	ethylpyrones A [b,c]	$C_{22}H_{26}O_8$	417.1555	13.15	0.429	3	
128.	ethylpyrones [b,c]	$C_{22}H_{26}O_9$	433.1504	13.46	−0.475	3	
129.	ethylpyrones [b,c]	$C_{24}H_{28}O_8$	443.1711	14.15	−0.341	3	
130.	isopropylpyrones [b,c]	$C_{23}H_{28}O_9$	447.1661	14.52	−0.147	3	
131.	methylpyrones (arenol)	$C_{21}H_{24}O_7$	387.1449	14.65	0.087	2	[25]
132.	ethylpyrones [b,c]	$C_{27}H_{34}O_8$	485.2181	14.89	0.472	3	
133.	unknown [b,c]	$C_{20}H_{26}O_6$	361.1657	15.07	0.937	3	
134.	ethylpyrones [b,c]	$C_{23}H_{28}O_9$	447.1661	15.23	−0.370	3	
135.	ethylpyrones (arzanol)	$C_{22}H_{26}O_7$	401.1606	15.76	−0.140	2	[25]

Table 1. *Cont.*

№	Identified/Tentatively Annotated Compound	Molecular Formula	Exact Mass [M-H]$^-$	t_R (min)	Δ ppm	Level of Confidence [21,29]	References
136.	ethylpyrones [b,c]	$C_{27}H_{34}O_8$	485.2181	15.81	0.101	3	
137.	ethylpyrones [b,c]	$C_{24}H_{30}O_9$	461.1817	16.30	0.012	3	
138.	ethylpyrones B [b,c]	$C_{25}H_{32}O_8$	459.2024	17.01	−0.307	3	
139.	isopropylpyrones [b,C]	$C_{23}H_{28}O_7$	415.1751	17.05	0.033	3	
140.	ethylpyrones [b,c]	$C_{22}H_{26}O_8$	417.1555	17.11	−0.146	3	
141.	ethylpyrones [b,c]	$C_{23}H_{28}O_7$	415.1751	17.81	0.177	3	
142.	ethylpyrone [b,c]	$C_{24}H_{28}O_8$	443.1711.	17.89	−0.476	2	
143.	1-methyl-propylpyrones [b,c]	$C_{24}H_{30}O_7$	429.1919	18.55	−0.458	3	
144.	isopropylpyrone [b,c]	$C_{23}H_{28}O_8$	431.1711	19.06	−0.489	3	
145.	unknown [b,c]	$C_{23}H_{32}O_6$	403.2126	19.22	0.128	3	
146.	ethylpyrones [b] (6-O-desmethyl-auricepyrone)	$C_{24}H_{30}O_7$	429.1919	19.57	−0.458	2	[24,27]
147.	ethylpyrones [b,c]	$C_{23}H_{28}O_8$	431.1711	19.86	−0.976	3	
148.	methylpyrones [b]	$C_{26}H_{32}O_7$	455.2075	20.19	0.513	3	[8,9,30]
149.	1-methyl-propylpyrones (heliarzanol/isobar)	$C_{24}H_{30}O_8$	445.1868	20.39	−0.744	3	
150.	1-methyl-propylpyrones [b,c]	$C_{24}H_{28}O_7$	427.1762	20.42	−5.914	3	
151.	ethylpyrones [b] (23-methyl-6-O-desmethylauricepyrone)	$C_{25}H_{32}O_7$	443.2075.	20.73	−0.060	3	[24,27]
152.	ethylpyrones (heliarzanol/isobar)	$C_{24}H_{30}O_8$	445.1868	21.00	−0.182	2	[8,9]
153.	ethylpyrones [b]	$C_{27}H_{34}O_7$	469.2232	21.23	0.050	2	[30]
154.	ethylpyrones B [b,c]	$C_{25}H_{32}O_8$	459.2024	21.67	0.368	3	
155.	ethylpyrones [b,c]	$C_{27}H_{34}O_8$	485.2181	21.97	−0.023	3	
156.	ethylpyrones C [b,c]	$C_{24}H_{28}O_7$	427.1762	22.13	0.102	2	
157.	isopropylpyrones [b]	$C_{28}H_{36}O_7$	483.2388	22.41	−0.055	3	[24]
158.	ethylpyrones C [b,c]	$C_{24}H_{28}O_7$	427.1762	23.01	−0.038	2	
Other compounds							
159.	gnaphaliol *O*-hexoside	$C_{19}H_{24}O_9$	395.1348	8.14	−6.316	2	[9]
160.	micropyrone	$C_{14}H_{20}O_4$	251.1289	9.12	−1.045	2	[8]
161.	Italipyrone 1	$C_{22}H_{24}O_7$	399.1449	17.33	−1.369	2	[9]
162.	Italipyrone 2	$C_{22}H_{24}O_7$	399.1449	20.39	−2.231	2	[9]
№	Identified/tentatively annotated compound	Molecular formula	Exact mass [M+H]$^+$	t_R (min)	Δ ppm	Level of confidence	References
163.	6-hydroxytremeton	$C_{13}H_{14}O_3$	219.1013	7.21	−1.373	3	[31]
164.	2-isobutyryl-6-acetylprenylphloroglucinol	$C_{17}H_{22}O_6$	323.1481	13.16	−2.522	3	[32]
165.	2-isobutyryl-4-prenylphloroglucinol	$C_{15}H_{20}O_4$	265.1431	17.68	−1.379	3	[32]
166.	2-metylvaleryl-4-prenylphloroglucinol	$C_{17}H_{24}O_4$	293.1741	18.28	−2.066	3	[32]

[a] Identified by comparison with an authentic standard; [b] reported for the first time in *H. italicum*; [c] -undescribed in the literature; A, B, and C compounds labeled with the same capital letters share the same fragmentation patterns; level of confidence: 1—compound identified by comparison to the reference standard; 2—putatively annotated compound; and 3—putatively characterized compound classes.

[M-H]$^-$ at *m/z* 417.156 (**127** and **140**), 431.171 (**147**), 445.187 (**152**), and 459.203 (**138** and **154**) indicated an additional oxygen atom than **135**, **141**, **146**, and **151**, respectively. The characteristic transitions in both negative and positive ion modes related to the losses of *m/z* 58.043 Da (C_3H_6O) and 72.058 Da (C_4H_8O) were employed to depict hydroxyprenyl residue. As an example, **147** with [M-H]$^-$ at *m/z* 431.171 (consistent with $C_{23}H_{27}O_8$) yielded

fragment ions at m/z 247.097 [M-H-$C_9H_{10}O_3$-H_2O]$^-$, 207.065 [M-H-$C_9H_{10}O_3$-C_3H_6O]$^-$, and 193.050 [M-H-$C_9H_{10}O_3$-C_4H_8O]$^-$ originating from the hydroxyprenyl moiety in the phloroglucinol skeleton (Figure S8). In (+) ESI-MS, the key points for the assignment of hydroxyprenyl moiety were the fragment ions at m/z 361.129 [M+H-C_4H_8O]$^+$, 189.055 [M+H-$C_8H_{10}O_3$-C_4H_8O]$^+$, and 177.054 [M+H-$C_9H_{10}O_3$-C_4H_8O]$^+$ together with the abundant ions at m/z 261.112 [M+H-$C_8H_{10}O_3$-H_2O]$^+$ (100%) and 249.112 [M+H-$C_9H_{10}O_3$-H_2O]$^+$ (90%). Additionally, prominent fragment ions at m/z 153.054 and 109.064 in (-) ESI/MS and 167.070 and 155.070 in (+) ESI/MS indicated an ethyl group at C-11 of the pyrone skeleton (Figure 4). The aforementioned structures are consistent with hydroxyprenyl residue at C-3, as was found in Heliarzanol [8,24]. It is worth noting that the 4-hydroxypyrone core exists in two tautomeric forms. On the other hand, the rotamers arise from the intramolecular hydrogen bonds between the oxygen functions of pyrone moiety and phenolic hydroxyl groups vicinal to the methylene bridge. Thus, different rotameric and/or tautomeric forms occur [8]. In the same way, hydroxyprenyl residue was evidenced in **138** and **154** ([M-H]$^-$ at m/z 459.203), where 2-methyl-oxobutyl residue at C-1 was deduced (Table S1).

MS data of **128** showed [M-H]$^-$ at 433.150 (consistent with $C_{22}H_{25}O_9$) (Table S1). In (-) ESI-MS, the precursor ion gave a base peak at m/z 267.087 [M-H-$C_9H_{10}O_3$]$^-$, indicating the same α-pyrone moiety as in arzanol (**135**) and a phloroglucinol unit with two oxygen atoms more than arzanol (Figure 4). The subsequent losses of 88.053 Da ($C_3H_6O_2$) and 74.038 Da ($C_4H_8O_2$) indicated the presence of a dihydroxylated prenyl unit. Accordingly, **128** yielded abundant fragment ions at m/z 223.0969 [M-H-$C_9H_{10}O_3$-CO_2]$^-$, 193.050 [M-H-$C_9H_{10}O_3$-$C_3H_6O_2$]$^-$, and 179.034 [M-H-$C_9H_{10}O_3$-$C_4H_8O_2$]$^-$, suggesting a hydroxyl group at both terminal C-19 and C-20 in the prenyl residue (Figure S8). This assumption was confirmed by the fragmentation pattern in (+) ESI-MS, where indicative ions at m/z 347.112 [M+H-$C_4H_8O_2$]$^+$, 193.0496 [M+H-$C_8H_{10}O_3$-$C_4H_8O_2$]$^+$, and 181.044 [M-H-$C_9H_{10}O_3$-$C_4H_8O_2$]$^-$ were generated (Figure S11). By analogy, compound **134** with [M-H]$^-$ at m/z 447.166 (calc. for $C_{23}H_{28}O_9$, -0.370 ppm) possessed an additional methylene group in the phloroglucinol unit in comparison with **128** and oxopropyl moiety at C-1. Compounds **128** and **134** were not reported in the literature.

MS/MS spectra of **153** with [M-H]$^-$ at m/z 469.223 was acquired (calc. for $C_{27}H_{33}O_7$)—there was a mass difference of 68 Da (C_5H_8) between its phloroglucinol moiety and that of arzanol (Tables S1 and S2). The prominent fragment ions at m/z 191.034 [M-H-$C_9H_{10}O_3$-C_8H_{16}]$^-$, 179.034 [M-H-$C_9H_{10}O_3$-C_9H_{16}]$^-$, and 166.026 [M-H-$C_9H_{10}O_3$-$C_{10}H_{17}$]$^-$ indicated a geranyl chain ($C_{10}H_{17}$) at C-3 instead of a prenyl one in arzanol (Table S1, Figure S8). This structure was consistent with the compound previously identified in *H. decumbens* [30]. The subsequent losses of 112.126 Da (C_8H_{16}), 124.126 Da (C_9H_{16}), and 137.134 Da ($C_{10}H_{17}$) are indicative of a geranyl unit. In the same way, the two compounds **136** and **155** with [M-H]$^-$ at m/z 485.218 (calc. for $C_{27}H_{33}O_8$) gave an abundant fragment ion at m/z 319.155 (72.4%) and the subsequent transitions 319.155→191.034, 319.155→179.034 and 319.155→166.026 indicating the losses of 128.121 Da ($C_8H_{16}O$), 140.121 Da ($C_9H_{16}O$), and 153.129 Da ($C_{10}H_{17}O$) (Table S1). Accordingly, hydroxygeranyl residue was suggested at C-3 of both pyrones.

An isopropyl group at C-11 was dedicated to compounds **130**, **139**, **144**, and **157** (Table S1, Figure S9). Concerning **139** ([M-H]$^-$ at m/z 415.176, calc. for $C_{23}H_{27}O_7$), the MS/MS spectrum afforded prominent fragment ions at m/z 247.097 [M-H-$C_9H_{12}O_3$]$^-$ and m/z 235.097 [M-H-$C_{10}H_{12}O_3$]$^-$, indicating an addition methylene group in the pyrone residue in comparison with **135** (arzanol). The presence of a prenyl moiety at C-3 was also evidenced by the abundant fragment ions at m/z 361.127 [M+H-C_4H_8]$^+$, 193.0496 [M+H-$C_{10}H_{12}O_3$-C_4H_8]$^+$, and 181.049 [M+H-$C_9H_{12}O_3$-C_4H_8]$^+$ in (+) ESI-MS. Thus, the isopropyl group was suggested at C-11, as was observed in Helitalone B [33] (Figure 4). The aforementioned compound is an isobar of compound Arenol B previously isolated from *H. oocephalum* [24]. The MS/MS spectra of **144** with [M-H]$^-$ at m/z 431.177 (calc. for $C_{23}H_{28}O_8$) and **130** with [M-H]$^-$ at m/z 447.166 (calc. for $C_{23}H_{28}O_9$) suggested one additional oxygen atom in **144** and two supplementary oxygen atoms in **130** in comparison with **139**, respectively. The

hydroxyprenyl moiety in **144** was dedicated from the indicative transitions in (+) ESI-MS 433.185→265.107→193.049 and 433.185→253.106→163.039 (Figure S11).

By analogy with **153**, geranyl moiety at C-3 of **157** [M-H]$^-$ at m/z 483.23, calc. for $C_{28}H_{36}O_7$) was evidenced, as was observed in achyroclinopyrone C, previously isolated from *H. oocephalum* [24] (Table S1).

Two compounds, **131** with [M-H]$^-$ at m/z 387.145 (calc. for $C_{21}H_{24}O_7$) and **148** with [M-H]$^-$ at m/z 455.208 (calc. for $C_{26}H_{32}O_7$), shared the same methylpyron moiety evidenced by the base peak [M-H-$C_8H_8O_3$]$^-$ at m/z 235.097 and 303.160, respectively (Table S1, Figure S7). The only difference was attributed to the occurrence of geranyl moiety ($C_{10}H_{17}$) in **148** instead of a prenyl moiety (C_5H_9) in **131**. In (+) ESI-MS/MS, **148** afforded abundant fragment ions at 333.090 [M+H-C_9H_{16}]$^+$ (52.3%) and 181.050 [M+H-(α-pyrone-C)-C_9H_{16}]$^-$ (100%), suggesting a geranyl moiety at C-3. Thus, **131** was consistent with arenal, previously identified in *H. italicum* [34], while **148** was ascribed as phloroglucinol pyron isolated from *H. decumbens* [30] (Figure 4).

The extracted ion chromatograms of prenylated phloroglucinol α-pyrones demonstrated that the *H. italicum* aerial parts' profile was dominated by arzanol (**135**) (19.28%), ethylpyrone **153** (11.34%), 6-*O*-desmethyl-auricepyrone (**146**) (10.72%), together with ethylpyrone **151** (8.14%), and isopropylpyrones (**139**) (5.30%) (Figure S6).
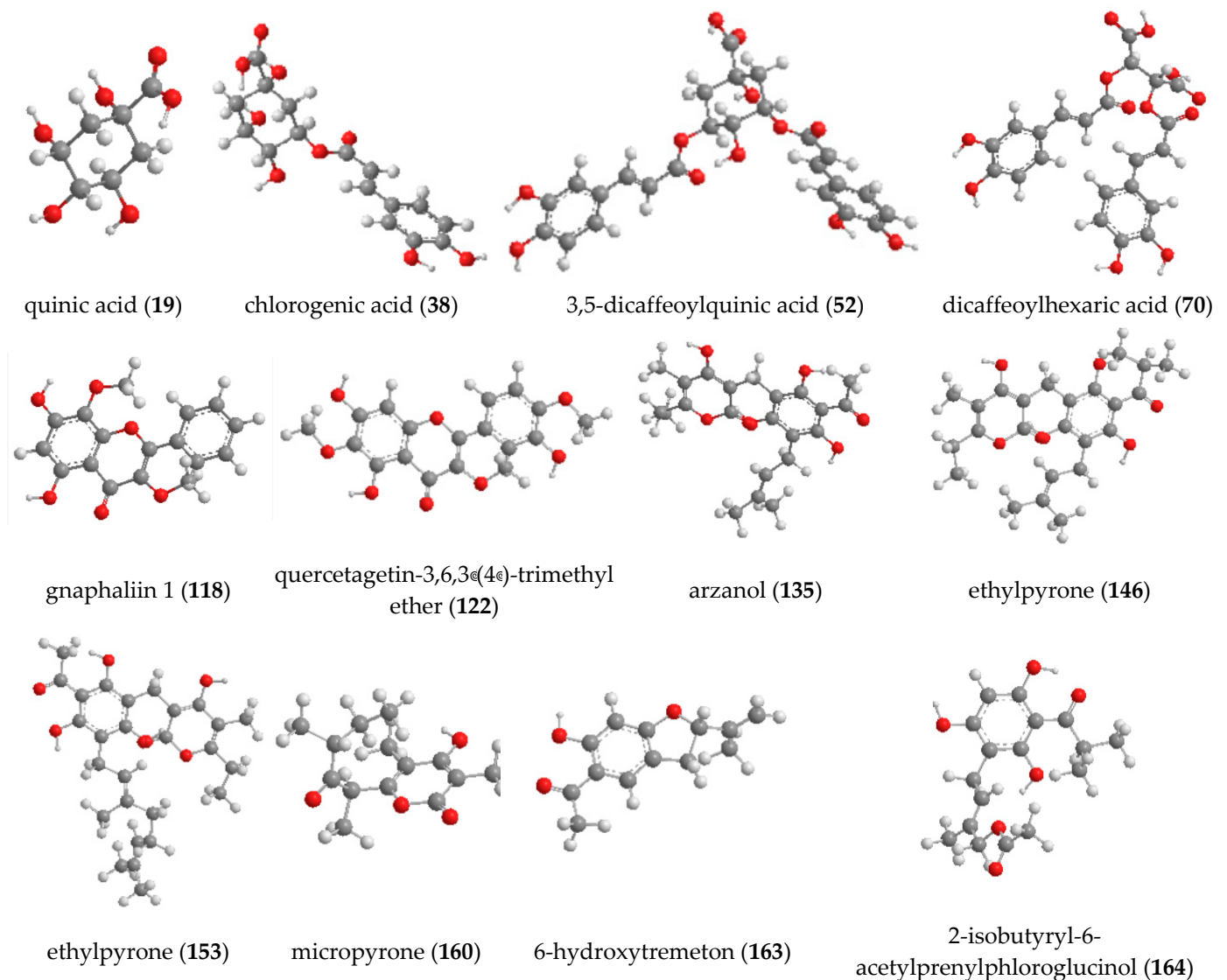
2.7. Other Compounds

The known monomer pyrone micropyrone **160** with [M-H]$^-$ at m/z 251.129 (calc. for $C_{14}H_{19}O_4$) was dereplicated together with italipirone and its isomer (**161**/**162**) consisting of both pyrone and a benzofurane ring [6]. A pyrone moiety was evidenced by the transition 399.144→233.0814 resulting from the loss of ethylpyrone as was observed in the heterodimer-pyrones (Table S1).

Four compounds were tentatively annotated in positive ion mode. Compound **163**, [M+H]$^+$ at m/z 219.101 ($C_{13}H_{14}O_3$), gave fragment ions at m/z 209.091 [M+H-H_2O]$^+$, 176.096 [M+H-H_2O-CO]$^+$, and 159.080 [M+H-H_2O-CO-CH_2]$^+$ and a base peak at m/z 183.080 [M+H-$2H_2O$]$^+$. Further fragmentation pathways of **163** consisted of the structure of 6-hydroxytremetone, previously isolated from *H. umbraculigerum* [31]. MS/MS spectrum of **165** ($C_{15}H_{20}O_4$) revealed consecutive losses of three OH groups at m/z 247.132 [M+H-H_2O]$^+$, m/z 191.070 [M+H-C_4H_8-H_2O]$^+$, and m/z 173.059 [M+H-C_4H_8-$2H_2O$]$^+$, consisting of the presence of a phloroglucinol skeleton. In addition, a base peak at m/z 209.080 [M+H-C_4H_8]$^+$, together with fragment ions at m/z 163.075 [M+H-C_4H_8-H_2O-CO]$^+$ and 135.080 [M+H-C_4H_8-H_2O-2CO]$^+$, were attributed to the structure of 2-isobutyryl-4-prenylphloroglucinol, previously found in *H. asperum*, *H. flanaganii*, *H. gymnocoum*, and *H. infaustum* [32]. Similar fragmentation pathways with losses of three OH groups, C_4H_8, and CO groups were presented in the MS/MS spectrum of **166** ($C_{17}H_{24}O_4$). Moreover, **164** differed from **165** with an additional methylene group (C_2H_4) and was tentatively annotated as 2-metylvaleryl-4-prenylphloroglucinol, isolated from *H. caespititium* [32]. In the same way, **164** gave a base peak at m/z 249.075 [M+H-H_2O-CO-C_4H_8]$^+$ and the subsequent fragment ions, corresponding to the losses of H_2O and CO groups. [M-H]$^-$ at m/z 323.148 (calc. for $C_{17}H_{22}O_6$) indicated 58 Da higher than that of **135**, suggesting additional acetyl moiety (Table S1). Compounds **164–166** belong to the groups of acylphloroglucinols. The predominant secondary metabolites among other compounds were micropyrone (**160**) (63.34%), followed by 6-hydroxytremeton (**163**) (14.15%) and 2-isobutyryl-6-acetylprenylphloroglucinol (**164**) (10.96%).

UHPLC-HRMS analysis revealed that phloroglucinol alpha-pyrones was the major group of secondary metabolites in *H. italicum* extract and reach up to 38.05% of all of the 166 compounds. Acylquinic acids (29.52%) and flavonoids (13.57%) were also found in high quantities in the studied species. Among all compounds, arzanol (**135**) (7.33%) was the predominant metabolite in the extract, while the amount of 3,4-dicaffeoylquinic acid (**51**), 3,5-dicaffeoylquinic acid (**52**), and 1,5-dicaffeoylquinic acid were found to be 5.61%, 5.58%,

and 4.58%, respectively. The structures of the main annotated metabolites in *H. italicum* extract are presented in Figure 5.

quinic acid (**19**)   chlorogenic acid (**38**)   3,5-dicaffeoylquinic acid (**52**)   dicaffeoylhexaric acid (**70**)

gnaphaliin 1 (**118**)   quercetagetin-3,6,3 (4)-trimethyl ether (**122**)   arzanol (**135**)   ethylpyrone (**146**)

ethylpyrone (**153**)   micropyrone (**160**)   6-hydroxytremeton (**163**)   2-isobutyryl-6-acetylprenylphloroglucinol (**164**)

Figure 5. Chemical structure of the main compounds in *H. italicum* extract.

## 2.8. Antioxidant and Cholinesterase Inhibitory Activity

In the present study, *H. italicum* extract was tested for antioxidant and cholinesterase inhibitory potential (Table 2). DPPH and ABTS+ were used to evaluate radical scavenging ability, while the reduction abilities were calculated by the CUPRAC, FRAP, and phospho-molybdenum (PHMD) methods. The metal chelating method was based on the binding of transition metals by phytochemicals. Results are presented as trolox equivalents and ethylenediaminetetraacetic acid (EDTA), and *H. italicum* extract revealed high activity of all of the used antioxidant methods. The enzyme inhibitory properties of *H. italicum* extracts were examined against both AChE and BChE. The results are calculated as a Galantamine (Gal) equivalent. The studied extract showed average AChE (1.64 ± 0.09 mg GALAE/g) and low BChE inhibitory potential (0.11 ± 0.02 mg GALAE/g). A high selectivity of the enzyme inhibitory activity of *H. italicum* extract targeting AChE was demonstrated.

Table 2. Antioxidant activity of *H. italicum* extract.

| Activity	Means $\pm$ SD
DPPH (mg TE/g)	110.33 ± 3.47
ABTS (mg TE/g)	234.70 ± 5.21
CUPRAC (mg TE/g)	354.23 ± 17.51
FRAP (mg TE/g)	210.24 ± 8.68
Chelating (mg EDTAE/g)	44.32 ± 0.75
Phosphomolybdenum (mmol TE/g)	1.97 ± 0.06

3. Passive Avoidance Test

In the passive avoidance test, the ability of the animals to learn the new task was assessed on the fifth day (Figure 6). On this day, only the group treated with the combination galantamine and *H. italicum* extract showed a slight increase in the latency time in comparison to the control and other groups. On day 12, when the memory of the animals was evaluated, groups treated with *Ginkgo biloba* and with the combination galantamine and *H. italicum* showed a statistically significant increase ($p \leq 0.001$) in the latency times compared to the control group (Figure 7). The result indicated an improvement of the memory processes after 12 days of administration of these compounds.
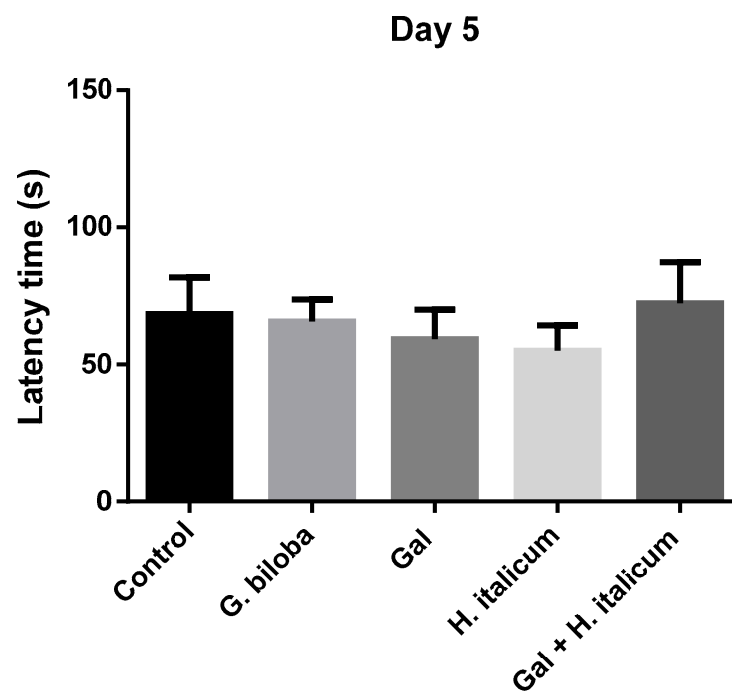
Figure 6. Effect of the compounds on the latency time on the 5th day of the administration. Results are presented as mean $\pm$ SEM. There are no statistically significant differences.

The incidence of dementia, a disease strongly associated with cognitive impairment, is on the rise globally with expectations that the number of patients will double every 20 years [35]. Early prevention of dementia is critical because no definitive therapy has been established. One of the promising sources for the prevention and treatment of different types of dementia, incl. Alzheimer's disease (AD), are plant sources [36]. In addition to evoking an antioxidant response, *H. italicum* essential oil also displays neuroprotective effects on mental fatigue/burnout, which generates further interest in *Helichrysum* extracts as potential cognitive-enhancing agents. Based on previous investigations, the *H. italicum* methanol–aqueous extract is worth investigating for the memory-ameliorating effects. We hypothesized that the combination of the *H. italicum* extract with the classical AChE inhibitor galantamine would support an improvement of the learning and memory process

in the behavioral test in mice. To consider this hypothesis, we used a passive avoidance test to investigate whether 12 days of per oral administration of the combination lead to an improvement of the memory processes in comparison to the control group, single drug, or plant extract application. Such a combination could be used in the future for the development of specific cognitive-enhancing formulations.
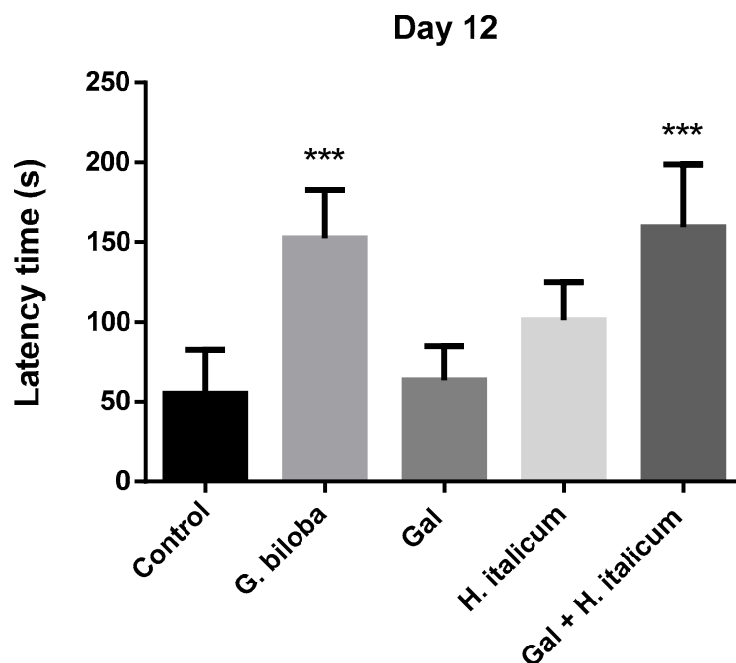
Figure 7. Effect of the compounds on the latency time on the 12th day of the administration. Results are presented as mean $\pm$ SEM. *** $p \leq 0.001$ statistically significant increase in the latency time in groups treated with *Ginkgo biloba* and Gal+ *H. italicum* extract in comparison to the control group.

When the mice were treated with the combination of galantamine (3 mg/kg) and *H. italicum* extract (200 mg/kg), a significant difference between combined and single applications was observed. It is worth noting that the combination was more beneficial for the memory-enhancement process in comparison with *G. biloba* (EGb 761) extract ($p \leq 0.001$) (Figure 6).

Taking into consideration that the antioxidant response is a key point in the memory-ameliorating effects, we proved the antioxidant activity of the *H. italicum* extract by chemical-based assays based on the scavenging activity toward a stable free radical (DPPH and ABTS), the reduction of metal ions (FRAP and CUPRAC), metal chelating, and total antioxidant potential [37]. The main mechanism by which antioxidants play their protective role included hydrogen atom transfer (HAT) or a single electron transfer (SET). Often, more complex reactions like mixed HAT/SET, stepwise electron transfer-proton transfer, concerted electron–proton transfer, or sequential proton loss electron transfer occur [38]. The studied *H. italicum* extract demonstrated strong radical scavenging, metal-reducing, and chelating activity. Taking into account that the DPPH scavenging activity depends on hydrogen atom transfer (HAT); the phenolic compounds (hydroxycinnamic and acylquinic acids, and flavonoids) are very active due to the lower bond dissociation energies (BDE) of the phenolic hydroxyl groups [39]. Consistent with already published studies, we confirm a positive correlation between these phenolic compounds' classes in *H. italicum* and the antioxidant potential [15]. On the other hand, *H. italicum* extract demonstrated a moderate inhibitory activity towards acetylcholinesterase.

In line with the aforementioned results, we suggest that the main phenolic compounds belonging to hydroxycinnamic caffeoylquinic and acylhexaric acids, phloroglucinol derivatives, and some flavonoids (luteolin, quercetin, pinocembrin, naringenin) in *H. italicum*

may hold significance for the memory enhancement observed in the passive avoidance test in mice.

Previously, caffeic, coumaric, and sinapic acids have been reported to improve cognitive function [40–42]. In different studies, the listed metabolites have been shown to suppress the breakdown of the amyloid-precursor protein, which is pathologically related to the Aβ (1–42) protein, lipid peroxidation, and neurite extension of hippocampal neurons [41,42]. These findings suggest that hydroxycinnamic acid intake may account for the improvement of the cognitive function, but the exact mechanism by which this intake affects cognitive function in humans is currently unknown. In the study of Kato et al. [43] on a small group of community-dwelling elderly individuals with complaints of subjective memory loss, after a 6-month intake period of caffeoylquinic acid there was significant improvement in attentional, executive, and memory functions.

Studies using mice and cultured neurons have shown that chlorogenic acid protect neurons and suppress the aggregation of amyloid beta (Aβ—one of the main hallmarks of AD) through antioxidant effects [41,44]. In addition, there are reports on beneficial effects of chlorogenic acid and/or its derivatives for ameliorating of spatial learning and memory and reducing behavioral deficits in a variety of in vivo animal models of disease or behavior [45].

Our previous study on *Achillea* species (Asteraceae family) has shown that the antioxidant activity of the species could be related to the synergetic action of metabolites such as 4-hydroxybenzoic acid-hexoside, 3-feruloylquinic acid, 1,3-dicaffeoylquinic acid, caffeic acid *O*-hexoside, 5-p-coumaroylquinic acid, and isorhamnetin 3-*O*-glucoside [12]. In this context, the bioinformatics analysis conducted through the platform Swiss Target Prediction confirmed that phenolic compounds, axillarin, quercetagetin-3,6,3′(4′)-trimethyl ether, quinic acid, dicaffeoylquinic acids, chlorogenic acid, and hesperetin could interact with target proteins, including hydrolase, electrochemical transporters, and transcription factors, involved in neuromodulation and neuroprotection [18].

Concerning flavones and flavonols, luteolin have been proved to exert a suppressive effect against endoplasmic reticulum stress activation and inflammatory signaling pathways in AD animal and cell models. Thus, the compound alleviates the learning and memory impairment in mice [46]. Numerous studies investigated the neuroprotective effects of quercetin in the central nervous system, especially in multiple in vitro and in vivo models of AD. Nakagawa et al. [47] reviewed seven studies of animal experiments estimating the neuroprotective effect of quercetin, in which quercetin improved cognition and memory deficits in rodent animal models of AD. The possible protective mechanisms of quercetin mainly involved the inhibition on Aβ aggregation and tauopathy, the anti-oxidative and anti-inflammatory activity, and amelioration of mitochondrial dysfunction [48].

A previous investigation demonstrated that the flavanone pinocembrin can be used to treat diseases such as stroke, AD, and vascular dementia [49,50]. Kang et al. revealed that pinocembrin attenuated learning and memory deficits induced by vascular dementia, by inducing the expression of Reelin, apoER2, and p-dab1 in the hippocampus. These authors also demonstrated that pinocembrin improved the impaired learning ability in rats by reducing the number of errors and decreasing the latency to step down in the step-down type of passive avoidance test [51]. Moreover, another flavanone naringenin dose dependently improved spatial recognition memory in Y maze, the discrimination ratio in a novel object discrimination task, and retention and recall capabilities in a passive avoidance test in the lipopolysaccharide-induced cognitive decline in rats. The authors suggested that naringenin have improved retention and recall in passive avoidance test via affecting synaptic plasticity [52]. Naringenin could ameliorate learning and memory deficit in passive avoidance tests in neurotoxic conditions through improvement of hippocampal oxidative stress and neuronal injury and increase the expression level of choline acetyltransferase [53].

It is worth noting that prenylated phloroglucinol α-pyrones and acylphloroglucinols could also attribute to the memory enhancing potential of *H. italicum* extract. It has been

found that phloroglucinol reduced oxidative stress induced by oligomeric Aβ1–42 (Aβ1–42) in the HT-22 hippocampal cell line. In addition, the reduction in dendritic spine density caused by either hydrogen peroxide or Aβ1–42 was significantly rescued by phloroglucinol in rat primary hippocampal neuron cultures. Furthermore, phloroglucinol attenuated memory deficits in the 5XFAD mouse model of AD based on the Morris water maze and T-maze tests. As a whole, phloroglucinol displays a therapeutic potential for AD patients as a ROS-scavenger [54].

Herein, the most prominent effect of memory was found in the group treated with *H. italicum* extract combined with galantamine. In our previous study, galantamine successfully reverses scopolamine-induced memory impairment in mice, especially on the 12th day [55]. A characteristic that makes galantamine appropriate for the treatment of AD is a selective inhibitory activity on the enzyme acetylcholinesterase (AChE) in the central nervous system with a small effect on peripheral tissues [56]. Subsequently to galantamine's approval for the treatment of mild-to-moderate AD in 2001, a wide variety of species have been assessed in pursuit of new AChE inhibitors [57]. Gonçalves et al. [58] reported that the methanol extract of *H. italicum*, rich with phenolic compounds (caffeoylquinic and dicaffeoylquinic acids, and pinocembrin), showed high inhibitory activity against enzymes involved in Alzheimer's disease like AChE, tyrosinase, and α-glucosidase.

Our results confirm the well-known positive effect of *G. biloba* extract on the memory processes. After 12 days of administration, the group treated with *G. biloba* (EGb 761) statistically significantly prolonged the latency time in the passive avoidance test in comparison to the control group. A standardized extract of *G. biloba* leaves EGb 761 is a popular dietary supplement taken to enhance mental focus and used for treatment of certain cerebral dysfunctions and dementias associated with aging and AD [59].

The extract EGb 761 is known to contain about 24% flavonoids and 6% terpene lactones. There is reliable evidence that standardized Ginkgo extract exhibits several molecular and cellular neuroprotective mechanisms, including attenuation of apoptosis, inhibition of membrane lipid peroxidation, anti-inflammatory effects, and direct inhibition of Aβ aggregation. There is also data showing that *G. biloba* extract significantly inhibits the activity of AChE in the brain [60]. The positive effects of EGb 761 on memory function, including in stress situations, have been demonstrated in many experiments involving mice, rats, and even chicks while using various tests and paradigms, including conventional passive and active avoidance, Morris water maze, scopolamine-induced amnesia, learned helplessness, and olfactory learning ability, etc. These studies involve acute or chronic treatment with EGb and highlight the positive effect concerns on short- or long-term memory [61].

4. Materials and Methods
4.1. Chemicals

Galantamine hydrobromide (Sopharma, Sofia, Bulgaria, Mw = 368.3 g/mol, purity > 98%); *Ginkgo biloba* capsules 80 mg (Adipharm, Sofia, Bulgaria, dry standardized leaf extract (EGb 761), contains 6% terpenolactones and 24% flavonoid glycosides).

Acetonitrile (hypergrade for LC-MS), formic acid (for LC-MS), and methanol (analytical grade) were purchased from Chromasolv (Sofia, Bulgaria). The reference standards used for compound identification were obtained from Extrasynthese (Genay, France) for protocatechuic, gentisic, *p*-coumaric, *m*-coumaric, o-coumaric, syringic, vanillic, and salicylic acids and hyperoside, luteolin 7-*O*-glucoside, isorhamnetin 3-*O*-glucoside, luteolin, quercetin, kaempferol, isorhamnetin, and jaceosidin. Neochlorogenic, chlorogenic, caffeic, 3,4-dicaffeoylquinic, 3,5-dicaffeoylquinic, and 1,5-dicaffeoylquinic acids were supplied from Phytolab (Vestenbergsgreuth, Germany).

4.2. Plant Material

H. italicum ssp. *italicum* aerial parts were collected in the full flowering stage in July 2022 at the Botanical Garden of Medicinal Plants (BGMP), Wroclaw Medical University,

Poland, and kindly supplied by Prof. Dr. Adam Matkowski. A voucher specimen was deposited at Herbarium Academiae Scientiarum Bulgariae (SOM 178 491). Subsequently, the plant material was dried at room temperature.

4.3. Sample Extraction

Air-dried powdered aerial parts (50 g) were extracted with 80% MeOH (1:20 *w/v*) by sonication (100 kHz, ultra-sound bath Biobase UC-20C) for 15 min (×2) at room temperature. Then, the methanol was evaporated in vacuo and water residues were lyophilized (lyophilizer Biobase BK-FD10P) to yield crude extract 1.38 g. Afterwards, the lyophilized extract was dissolved in 80% methanol (0.1 mg/mL), filtered through a 0.45 μm syringe filter (Polypure II, Alltech, Lokeren, Belgium), and an aliquot (2 mL) of each solution was subjected to UHPLC–HRMS analyses. The same extract was used for further in vitro and in vivo tests.

4.4. UHPLC-HRMS Profiling

The phytochemical analyses were performed on a Q Exactive Plus mass spectrometer (ThermoFisher Scientific, Inc. Walthham, USA). The apparatus operated in negative and positive modes in *m/z* range from 100 to 1000. The chromatographic separation was performed on a reversed phase column Kromasil EternityXT C18 (1.8 μm, 2.1 × 100 mm) at 40 °C. The chromatographic analyses were performed as previously described [14]. Separation was achieved on an UHPLC system Dionex Ultimate 3000RSLC (ThermoFisher Scientific, Inc.) The mobile phase consisted of A: water (with 0.1% formic acid) and B: acetonitrile (with 0.1% formic acid). The used gradient was as follows: 5% B for 1 min, gradually turned to 30% B over 19 min, increased gradually to 50% B over 5 min, increased gradually to 70% B over 5 min, and finally increased gradually to 95% over 3 min. The system was then turned to the initial condition and equilibrated over 4 min. The flow rate was 300 μL/min and the injection volume was 1 μL. Data acquisition and processing were performed with Xcalibur 4.2 software (ThermoScientific, Walthham, USA). Peaks annotations were based on accurate masses in full MS and ddMS2, MS/MS fragmentation pathways, precursor and fragment ions relative abundance, elemental composition, comparison with the retention times, fragment spectra, and chromatographic behavior of reference standards obtained from an in-house database of previously identified compounds. The compounds identified with reference standards during the present study belong to confidence class 1, while the compounds that were putatively annotated belong to level 2 (reported in *H. italicum* previously), and putatively characterized classes belong to level 3 [29].

MZmine 2 software was applied to the UHPLC–HRMS raw files of the studied *H. italicum* extracts for the semi-quantitative analysis. Results are expressed as the % peak area of the compound to the total peak areas of the corresponding group secondary metabolites and all metabolites.

4.5. Antioxidant and Enzyme Inhibitory Assays

DPPH radical scavenging assay: The dsample solution (1 mg/mL; 1 mL) was added to 4 mL of a 0.004% methanol solution of DPPH. The sample absorbance was measured at 517 nm after a 30 min incubation [62].

ABTS radical scavenging assay: Briefly, ABTS+ was produced by reacting 7 mM ABTS solution with 2.45 mM potassium persulfate and allowing the mixture to stand for 12–16 h in the dark at room temperature. The ABTS solution was diluted with methanol to an absorbance of 0.700 ± 0.02 at 734 nm. The sample solution (1 mg/mL; 1 mL) was added to the ABTS solution (2 mL) and mixed. The sample absorbance was measured at 734 nm after a 30 min incubation at room temperature [62].

CUPRAC assay: The sample solution (1 mg/mL; 0.5 mL) was added to the reaction mixture containing $CuCl_2$ (1 mL, 10 mM), neocuproine (1 mL, 7.5 mM), and NH_4Ac buffer (1 mL, 1 M, pH 7.0). Similarly, a blank was prepared without $CuCl_2$. Then, the sample and

blank absorbances were measured at 450 nm after a 30 min incubation at room temperature. The absorbance of the blank was subtracted from that of the sample [62].

FRAP (ferric reducing antioxidant power) activity assay: The sample solution (1 mg/mL; 0.1 mL) was added to premixed FRAP reagent (2 mL) containing acetate buffer, 2,4,6-tris(2-pyridyl)-S-triazine (TPTZ) (10 mM) in 40 mM HCl and ferric chloride (20 mM) in a ratio of 10:1:1 (*v/v/v*). Then, the sample absorbance was read at 593 nm after a 30 min incubation at room temperature. DPPH, ABTS, CUPRAC, and FRAP activity were expressed as milligrams of trolox equivalents (mg TE/g extract) [62].

Metal chelating activity assay: Briefly, the sample solution (1 mg/mL; 2 mL) was added to FeCl2 solution (0.05 mL, 2 mM). The reaction was initiated by the addition of 5 mM ferrozine (0.2 mL). Similarly, a blank was prepared without ferrozine. Then, the sample and blank absorbances were measured at 562 nm after 10 min incubation at room temperature. The metal chelating activity was expressed as milligrams of EDTA (disodium edetate) equivalents (mg EDTAE/g extract) [62].

Phosphomolybdenum method: The sample solution (1 mg/mL; 0.3 mL) was mixed with 3 mL of reagent solution (0.6 M sulfuric acid, 28 mM sodium phosphate and 4 mM ammonium molybdate). The sample absorbance was measured at 695 nm after a 90 min incubation at 95 °C. The total antioxidant capacity was expressed as millimoles of trolox equivalents (mmol TE/g extract) [62].

Cholinesterase inhibitory activity assay: The sample solution (1 mg/mL; 50 μL) was mixed with DTNB (5,5-dithio-bis(2-nitrobenzoic) acid, Sigma, St. Louis, MO, USA), (125 μL) and AChE (acetylcholines-terase (Electric ell AChE, Type-VI-S, EC 3.1.1.7, Sigma)), or BChE (BChE (horse serum BChE, EC 3.1.1.8, Sigma, Burlington, MA, USA)) solution (25 μL) in Tris–HCl buffer (pH 8.0) in a 96-well microplate and incubated for 15 min at 25 °C. The reaction was then initiated with the addition of acetylthiocholine iodide (ATCI, Sigma) or butyrylthiocholine chloride (BTCl, Sigma) (25 μL). Similarly, a blank was prepared by adding the sample solution to all reaction reagents without an enzyme (AChE or BChE) solution. The sample and blank absorbances were read at 405 nm after 10 min incubation at 25 °C. The absorbance of the blank was subtracted from that of the sample, and the cholinesterase inhibitory activity was expressed as galanthamine equivalents (mgGALAE/g extract).

4.6. Animals

The experiment was conducted on 30 male mice, line H, with a body weight in the range of 28–32 g. All experiments were approved by the Institutional Animal Care Committee at the Medical University of Sofia. The animals were divided into 5 groups (n = 6). The tested substances were administered perorally (p.o.) in the following doses:

Group 1: control group, receiving distilled water only;
Group 2: animals treated with *H. italicum* extract—200 mg/kg;
Group 3: animals treated with galantamine—3 mg/kg;
Group 4: animals treated with *Ginkgo biloba* (EGB761)—100 mg/kg;
Group 5: animals treated with galantamine (3 mg/kg) and *H. italicum* extract—200 mg/kg.

The substances were in a solid form; they were ground, and the required amount of distilled water was added.

All treatments were performed for 12 days. During this period, animals were observed daily for behavioral changes and signs of toxicity. The experiment was conducted in accordance with the Directive 2010/63/EU of the European Parliament and of the Council on the protection of animals used for scientific purposes (No. 346 of 28 February 2023) from the Bulgarian Food Safety Agency.

4.7. Passive Avoidance Test

The learning and memory processes of the experimental mice were evaluated by a passive avoidance test using an automated shuttle box (Gemini Avoidance System, San Diego Instruments). The apparatus consists of two identical compartments (25 × 20 × 16 cm each)

with an electrified grid floor. The chambers are separated by a wall with a guillotine door (8×6 cm). The test started with an acclimatization period of 20 s. The maximum duration of the trial was 300 s. If a mouse entered the dark chamber, a weak electric shock with an intensity of 0.5 mA and a duration of 3 s. was applied through the grid floor. Learning was assessed by the latency of entry into the dark compartment. An increase in latency time indicated an improvement of the learning and memory processes. The tested compounds were administered p.o. 1 h before passive avoidance testing on days 1–5 of the experiment and then daily for 7 days without testing in the apparatus. On the 12th day the memory storage, processes were evaluated again by passive avoidance test.

4.8. Statistical Analysis

The results from the passive avoidance test were processed statistically using Graph-Pad Prism 6 software and presented as mean $\pm$ SEM. The groups were compared using one-way ANOVA followed by a post-hoc comparison of sample means (Tukey test). The differences were considered statistically significant at $p \leq 0.05$.

5. Conclusions

For the first time, more than 90 secondary metabolites were reported in *H. italicum* including phenylethanoid glycosides, a series of hydroxybenzoic and hydroxicinnamic acid–glycosides, caffeoyl-hydroxydihydrocaffeoylquinic, *p*-coumaroyl-caffeoylquinic and tricaffeoylquinic acids, malonyl-dicaffeoylquinic acids, a series of caffeoylhexaric acids, and methoxylated derivatives of scutelarein, quercetagetin, and 6-hydroxyluteolin. The main finding of the phytochemical study was a comprehensive profiling of heterodimer-pyrones where 23 compounds, undescribed in the literature, were annotated. This study is the first attempt to propose the fragmentation patterns of four subclasses pyrones in LC-HRMS. For the first time, the cognitive-enhancing properties of *H. italicum* extract is reported. We have demonstrated that the combination of the extract and classical acetylcholinesterase inhibitor galantamine significantly improved the learning and memory after 12 days administration in a passive avoidance test in mice. The effect is more pronounced even than that of *G. biloba* (EGb 761). Taken together, our data suggest significant antioxidant activity of *H. italicum* extract by radical scavenging activity, reducing power and metal chelating capacity. The extract showed moderate acetylcholinesterase and low butyrylcholinesterase inhibitory potential. It appears that powerful antioxidant activity coupled with moderate and selective AChE inhibitory ability accounted for the cognitive-enhancing potential of *H. italicum* extract. Prenylated phloroglucinol derivatives, acylquinic and acylhexaric acids, and flavonoids may hold significance for the memory improvement potential of *H. italicum* extract. Further analysis concerning mechanisms of action is needed to advance our knowledge on the pharmacological effects of *H. italicum*.

extract. Table S2. Tentative structures of prenylated phloroglucinol α-pyrones (for numbers and fragmentation patterns, see Table S1).

References

1. Ninčević, T.; Grdiša, M.; Šatović, Z.; Jug-Dujaković, M. *Helichrysum italicum* (Roth) G. Don: Taxonomy, biological activity, biochemical and genetic diversity. *Ind. Crops Prod.* **2019**, *138*, 111487. [CrossRef]

2. Viegas, D.A.; Palmeira-de-Oliveira, A.; Salgueiro, L.; Martinez-de-Oliveira, J.; Palmeira-de-Oliveira, R. *Helichrysum italicum*: From traditional use to scientific data. *J. Ethnopharmacol.* **2014**, *151*, 54–65. [CrossRef]

3. Perrini, R.; Morone-Fortunato, I.; Lorusso, E.; Avato, P. Glands, essential oils and in vitro establishment of *Helichrysum italicum* (Roth) G. Don ssp. *microphyllum* (Willd.) Nyman. *Ind. Crops Prod.* **2009**, *29*, 395–403. [CrossRef]

4. Akaberi, M.; Sahebkar, A.; Azizi, N.; Emami, S.A. Everlasting flowers: Phytochemistry and pharmacology of the genus *Helichrysum*. *Ind. Crops Prod.* **2019**, *138*, 111471. [CrossRef]

5. Maksimovic, S.; Tadic, V.; Skala, D.; Zizovic, I. Separation of phytochemicals from *Helichrysum italicum*: An analysis of different isolation techniques and biological activity of prepared extracts. *Phytochemistry* **2017**, *138*, 9–28. [CrossRef]

6. Fraternale, D.; Flamini, G.; Ascrizzi, R. In vitro anticollagenase and antielastase activities of essential oil of *Helichrysum italicum* subsp. *italicum* (Roth) G. Don. *J. Med. Food* **2019**, *22*, 1041–1046. [CrossRef]

7. Bianchini, A.; Tomi, P.; Costa, J.; Bernardini, A.F. Composition of *Helichrysum italicum* (Roth) G. Don fil. subsp. *italicum* essential oils from Corsica (France). *Flavour Fragr. J.* **2001**, *16*, 30–34. [CrossRef]

8. Taglialatela-Scafati, O.; Pollastro, F.; Chianese, G.; Minassi, A.; Gibbons, S.; Arunotayanun, W.; Mabebie, B.; Ballero, M.; Appendino, G. Antimicrobial phenolics and unusual glycerides from *Helichrysum italicum* subsp. *microphyllum*. *J. Nat. Prod.* **2013**, *76*, 346–353. [CrossRef]

9. Kramberger, K.; Barlič-Maganja, D.; Bandelj, D.; Baruca Arbeiter, A.; Peeters, K.; Miklavčič Višnjevec, A.; Jenko Pražnikar, Z. HPLC-DAD-ESI-QTOF-MS determination of bioactive compounds and antioxidant activity comparison of the hydroalcoholic and water extracts from two *Helichrysum italicum* species. *Metabolites* **2020**, *10*, 403. [CrossRef]

10. Kramberger, K.; Kenig, S.; Jenko Pražnikar, Z.; Kočevar Glavač, N.; Barlič-Maganja, D. A review and evaluation of the data supporting internal use of *Helichrysum italicum*. *Plants* **2021**, *10*, 1738. [CrossRef]

11. Allard, P.-M.; Genta-Jouve, G.; Wolfender, J.-L. Deep metabolome annotation in natural products research: Towards a virtuous cycle in metabolite identification. *Curr. Opin. Chem. Biol.* **2017**, *36*, 40–49. [CrossRef]

12. Terracina, S.; Ferraguti, G.; Petrella, C.; Bruno, S.M.; Blaconà, G.; Di Certo, M.G.; Minni, A.; Greco, A.; Musacchio, A.; Ralli, M. Characteristic Hallmarks of Aging and the Impact on Carcinogenesis. *Curr. Cancer Drug Targets* **2023**, *23*, 87–102.

13. Shu, Y.; Zou, C.; Cai, Y.; He, Q.; Wu, X.; Zhu, H.; Qv, M.; Chao, Y.; Xu, C.; Tang, L. Vitamin C deficiency induces hypoglycemia and cognitive disorder through S-nitrosylation-mediated activation of glycogen synthase kinase 3β. *Redox Biol.* **2022**, *56*, 102420. [CrossRef]

14. Fiore, M.; Messina, M.P.; Petrella, C.; D'Angelo, A.; Greco, A.; Ralli, M.; Ferraguti, G.; Tarani, L.; Vitali, M.; Ceccanti, M. Antioxidant properties of plant polyphenols in the counteraction of alcohol-abuse induced damage: Impact on the Mediterranean diet. *J. Funct. Foods* **2020**, *71*, 10401. [CrossRef]

15. Węglarz, Z.; Kosakowska, O.; Pióro-Jabrucka, E.; Przybył, J.L.; Gniewosz, M.; Kraśniewska, K.; Szyndel, M.S.; Costa, R.; Bączek, K.B. Antioxidant and antibacterial activity of *Helichrysum italicum* (Roth) G. Don. from central Europe. *Pharmaceuticals* **2022**, *15*, 735. [CrossRef]

16. Kenig, S.; Kramberger, K.; Petelin, A.; Bandelj, D.; Baruca Arbeiter, A.; Miklavčič Višnjevec, A.; Peeters, K.; Mohorko, N.; Šik Novak, K.; Jenko Pražnikar, Z. Helichrysum italicum ssp. *italicum* infusion promotes fat oxidation in hepatocytes and stimulates energy expenditure and fat oxidation after acute ingestion in humans: A pilot study. *Plants* **2021**, *10*, 1516. [CrossRef]

17. Varney, E.; Buckle, J. Effect of inhaled essential oils on mental exhaustion and moderate burnout: A small pilot study. *J. Altern. Complement. Med.* **2013**, *19*, 69–71. [CrossRef]

18. Ak, G.; Gevrenova, R.; Sinan, K.I.; Zengin, G.; Zheleva, D.; Mahomoodally, M.F.; Senkardes, I.; Brunetti, L.; Leone, S.; Di Simone, S.C. *Tanacetum vulgare* L.(Tansy) as an effective bioresource with promising pharmacological effects from natural arsenal. *Food Chem. Toxicol.* **2021**, *153*, 112268. [CrossRef]

19. Gevrenova, R.; Zengin, G.; Sinan, K.I.; Yıldıztugay, E.; Zheleva-Dimitrova, D.; Picot-Allain, C.; Mahomoodally, M.F.; Imran, M.; Dall'Acqua, S. UHPLC-MS Characterization and biological insights of different solvent extracts of two *Achillea* species (A. aleppica and A. santolinoides) from Turkey. *Antioxidants* **2021**, *10*, 1180. [CrossRef]

20. Gevrenova, R.; Zengin, G.; Sinan, K.I.; Zheleva-Dimitrova, D.; Balabanova, V.; Kolmayer, M.; Voynikov, Y.; Joubert, O. An in-Depth study of metabolite profile and biological potential of *Tanacetum balsamita* L. (Costmary). *Plants* **2022**, *12*, 22. [CrossRef]

21. Gevrenova, R.; Zheleva-Dimitrova, D.; Balabanova, V.; Voynikov, Y.; Sinan, K.I.; Mahomoodally, M.F.; Zengin, G. Integrated phytochemistry, bio-functional potential and multivariate analysis of *Tanacetum macrophyllum* (Waldst. & Kit.) Sch. Bip. and *Telekia speciosa* (Schreb.) Baumg. (Asteraceae). *Ind. Crops Prod.* **2020**, *155*, 112817.

22. Kłeczek, N.; Michalak, B.; Malarz, J.; Kiss, A.K.; Stojakowska, A. *Carpesium divaricatum* Sieb. & Zucc. revisited: Newly identified constituents from aerial parts of the plant and their possible contribution to the biological activity of the Plant. *Molecules* **2019**, *24*, 1614.

23. Cuyckens, F.; Claeys, M. Mass spectrometry in the structural analysis of flavonoids. *J. Mass Spectrom.* **2004**, *39*, 1–15. [CrossRef]

24. Akaberi, M.; Danton, O.; Tayarani-Najaran, Z.; Asili, J.; Iranshahi, M.; Emami, S.A.; Hamburger, M. HPLC-based activity profiling for antiprotozoal compounds in the endemic Iranian medicinal plant *Helichrysum oocephalum*. *J. Nat. Prod.* **2019**, *82*, 958–969. [CrossRef]

25. Appendino, G.; Ottino, M.; Marquez, N.; Bianchi, F.; Giana, A.; Ballero, M.; Sterner, O.; Fiebich, B.L.; Munoz, E. Arzanol, an anti-inflammatory and anti-HIV-1 phloroglucinol α-pyrone from *Helichrysum italicum* ssp. *microphyllum*. *J. Nat. Prod.* **2007**, *70*, 608–612. [CrossRef]

26. Pereira, C.G.; Barreira, L.; Bijttebier, S.; Pieters, L.; Neves, V.; Rodrigues, M.J.; Rivas, R.; Varela, J.; Custodio, L. Chemical profiling of infusions and decoctions of *Helichrysum italicum* subsp. *picardii* by UHPLC-PDA-MS and in vitro biological activities comparatively with green tea (*Camellia sinensis*) and rooibos tisane (*Aspalathus linearis*). *J. Pharm. Biomed. Anal.* **2017**, *145*, 593–603. [CrossRef]

27. Jakupovic, J.; Kuhnke, J.; Schuster, A.; Metwally, M.; Bohlmann, F. Phloroglucinol derivatives and other constituents from South African *Helichrysum* species. *Phytochemistry* **1986**, *25*, 1133–1142. [CrossRef]

28. Mutanyatta-Comar, J.; Phale, O.; Abegaz, B.; Croft, K. Phloroglucinol derivatives and flavones from *Helichrysum paronychioides*. *Bull. Chem. Soc. Ethiop.* **2006**, *20*, 61–68.

29. Sumner, L.W.; Amberg, A.; Barrett, D.; Beale, M.H.; Beger, R.; Daykin, C.A.; Fan, T.W.-M.; Fiehn, O.; Goodacre, R.; Griffin, J.L. Proposed minimum reporting standards for chemical analysis: Chemical analysis working group (CAWG) metabolomics standards initiative (MSI). *Metabolomics* **2007**, *3*, 211–221. [CrossRef]

30. Tomás-Lorente, F.; Iniesta-Sanmartín, E.; Tomás-Barberán, F.A.; Trowitzsch-Kienast, W.; Wray, V. Antifungal phloroglucinol derivatives and lipophilic flavonoids from *Helichrysum decumbens*. *Phytochemistry* **1989**, *28*, 1613–1615. [CrossRef]

31. Bohlmann, F.; Hoffmann, E. Cannabigerol-ähnliche verbindungen aus *Helichrysum umbraculigerum*. *Phytochemistry* **1979**, *18*, 1371–1374. [CrossRef]

32. Lourens, A.; Viljoen, A.M.; Van Heerden, F. South African *Helichrysum* species: A review of the traditional uses, biological activity and phytochemistry. *J. Ethnopharmacol.* **2008**, *119*, 630–652. [CrossRef]

33. Werner, J.; Ebrahim, W.; Özkaya, F.C.; Mándi, A.; Kurtán, T.; El-Neketi, M.; Liu, Z.; Proksch, P. Pyrone derivatives from *Helichrysum italicum*. *Fitoterapia* **2019**, *133*, 80–84. [CrossRef]

34. Vrkoč, J.; Dolejš, L.; Sedmera, P.; Vašíčková, S.; Šorm, F. The structure of arenol and homoarenol, α-pyrone derivatives from *Helichrysum arenarium* (L.) Moench. *Tetrahedron Lett.* **1971**, *12*, 247–250. [CrossRef]

35. Prince, M.; Wimo, A.; Guerchet, M.; Ali, G.-C.; Wu, Y.-T.; Prina, M. World Alzheimer report 2015. In *The Global Impact of Dementia: An Analysis of Prevalence, Incidence, Cost and Trends*; Alzheimer's Disease International: London, UK, 2015.

36. John, O.O.; Amarachi, I.S.; Chinazom, A.P.; Adaeze, E.; Kale, M.B.; Umare, M.D.; Upaganlawar, A.B. Phytotherapy: A promising approach for the treatment of Alzheimer's disease. *Pharmacol. Res.-Mod. Chin. Med.* **2022**, *2*, 100030. [CrossRef]

37. Rumpf, J.; Burger, R.; Schulze, M. Statistical evaluation of DPPH, ABTS, FRAP, and Folin-Ciocalteu assays to assess the antioxidant capacity of lignins. *Int. J. Biol. Macromol.* **2023**, *233*, 123470. [CrossRef]

38. Ilyasov, I.R.; Beloborodov, V.L.; Selivanova, I.A.; Terekhov, R.P. ABTS/PP decolorization assay of antioxidant capacity reaction pathways. *Int. J. Mol. Sci.* **2020**, *21*, 1131. [CrossRef]

39. Bendary, E.; Francis, R.; Ali, H.; Sarwat, M.; El Hady, S. Antioxidant and structure–activity relationships (SARs) of some phenolic and anilines compounds. *Ann. Agric. Sci.* **2013**, *58*, 173–181. [CrossRef]

40. Farah, A.; Monteiro, M.; Donangelo, C.M.; Lafay, S. Chlorogenic acids from green coffee extract are highly bioavailable in humans. *J. Nutr.* **2008**, *138*, 2309–2315. [CrossRef]

41. Ito, H.; Sun, X.-L.; Watanabe, M.; Okamoto, M.; Hatano, T. Chlorogenic acid and its metabolite m-coumaric acid evoke neurite outgrowth in hippocampal neuronal cells. *Biosci. Biotechnol. Biochem.* **2008**, *72*, 885–888. [CrossRef]

42. Lee, H.E.; Kim, D.H.; Park, S.J.; Kim, J.M.; Lee, Y.W.; Jung, J.M.; Lee, C.H.; Hong, J.G.; Liu, X.; Cai, M. Neuroprotective effect of sinapic acid in a mouse model of amyloid β1–42 protein-induced Alzheimer's disease. *Pharmacol. Biochem. Behav.* **2012**, *103*, 260–266. [CrossRef]

43. Kato, M.; Ochiai, R.; Kozuma, K.; Sato, H.; Katsuragi, Y. Effect of chlorogenic acid intake on cognitive function in the elderly: A pilot study. *Evid.-Based Complement. Altern. Med.* **2018**, *2018*, 8608497. [CrossRef]

44. Kwon, S.-H.; Lee, H.-K.; Kim, J.-A.; Hong, S.-I.; Kim, H.-C.; Jo, T.-H.; Park, Y.-I.; Lee, C.-K.; Kim, Y.-B.; Lee, S.-Y. Neuroprotective effects of chlorogenic acid on scopolamine-induced amnesia via anti-acetylcholinesterase and anti-oxidative activities in mice. *Eur. J. Pharmacol.* **2010**, *649*, 210–217. [CrossRef]

45. Cropley, V.; Croft, R.; Silber, B.; Neale, C.; Scholey, A.; Stough, C.; Schmitt, J. Does coffee enriched with chlorogenic acids improve mood and cognition after acute administration in healthy elderly? A pilot study. *Psychopharmacology* **2012**, *219*, 737–749. [CrossRef]

46. Kou, J.-j.; Shi, J.-z.; He, Y.-y.; Hao, J.-j.; Zhang, H.-y.; Luo, D.-m.; Song, J.-k.; Yan, Y.; Xie, X.-m.; Du, G.-h. Luteolin alleviates cognitive impairment in Alzheimer's disease mouse model via inhibiting endoplasmic reticulum stress-dependent neuroinflammation. *Acta Pharmacol. Sin.* **2022**, *43*, 840–849. [CrossRef]

47. Nakagawa, T.; Ohta, K. Quercetin regulates the integrated stress response to improve memory. *Int. J. Mol. Sci.* **2019**, *20*, 2761. [CrossRef]

48. Zhang, X.-W.; Chen, J.-Y.; Ouyang, D.; Lu, J.-H. Quercetin in animal models of Alzheimer's disease: A systematic review of preclinical studies. *Int. J. Mol. Sci.* **2020**, *21*, 493. [CrossRef]

49. Qin, L.; Tu, W.; Sun, X.; Zhang, J.; Chen, Y.; Zhao, H. Retardation of neurobehavioral development and reelin down-regulation regulated by further DNA methylation in the hippocampus of the rat pups are associated with maternal deprivation. *Behav. Brain Res.* **2011**, *217*, 142–147. [CrossRef]

50. Rogers, J.T.; Rusiana, I.; Trotter, J.; Zhao, L.; Donaldson, E.; Pak, D.T.; Babus, L.W.; Peters, M.; Banko, J.L.; Chavis, P. Reelin supplementation enhances cognitive ability, synaptic plasticity, and dendritic spine density. *Learn. Mem.* **2011**, *18*, 558–564. [CrossRef]

51. Kang, Z.-C.; Wang, H.-G.; Yang, Y.-L.; Zhao, X.-Y.; Zhou, Q.-M.; Yang, Y.-L.; Yang, J.-Y.; Du, G.-H. Pinocembrin ameliorates cognitive impairment induced by vascular dementia: Contribution of Reelin-dab1 signaling pathway. *Drug Des. Dev. Ther.* **2020**, *14*, 3577–3587. [CrossRef]

52. Khajevand-Khazaei, M.-R.; Ziaee, P.; Motevalizadeh, S.-A.; Rohani, M.; Afshin-Majd, S.; Baluchnejadmojarad, T.; Roghani, M. Naringenin ameliorates learning and memory impairment following systemic lipopolysaccharide challenge in the rat. *Eur. J. Pharmacol.* **2018**, *826*, 114–122. [CrossRef]

53. Khan, M.B.; Khan, M.M.; Khan, A.; Ahmed, M.E.; Ishrat, T.; Tabassum, R.; Vaibhav, K.; Ahmad, A.; Islam, F. Naringenin ameliorates Alzheimer's disease (AD)-type neurodegeneration with cognitive impairment (AD-TNDCI) caused by the intracerebroventricular-streptozotocin in rat model. *Neurochem. Int.* **2012**, *61*, 1081–1093. [CrossRef]

54. Yang, E.-J.; Ahn, S.; Ryu, J.; Choi, M.-S.; Choi, S.; Chong, Y.H.; Hyun, J.-W.; Chang, M.-J.; Kim, H.-S. Phloroglucinol attenuates the cognitive deficits of the 5XFAD mouse model of Alzheimer's disease. *PLoS ONE* **2015**, *10*, e0135686. [CrossRef]

55. Kostadinova, I.; Danchev, N.; Vezenkov, L.; Tsekova, D.; Rozhanets, V. Effect of Original Peptide Derivatives of Galantamine on Passive Avoidance in Mice. *Bull. Exp. Biol. Med.* **2020**, *170*, 200–202. [CrossRef]

56. Marucci, G.; Buccioni, M.; Dal Ben, D.; Lambertucci, C.; Volpini, R.; Amenta, F. Efficacy of acetylcholinesterase inhibitors in Alzheimer's disease. *Neuropharmacology* **2021**, *190*, 108352. [CrossRef]

57. Coelho dos Santos, T.; Gomes, T.; Pinto, B.; Camara, A.; Antonio de Andrade Paes, M. Naturally Occurring Acetylcholinesterase Inhibitors and Their Potential Use for Alzheimer's Disease. *Ther. Front. Pharmacol.* **2018**, *9*, 1192. [CrossRef]

58. Gonçalves, S.; Moreira, E.; Grosso, C.; Andrade, P.B.; Valentão, P.; Romano, A. Phenolic profile, antioxidant activity and enzyme inhibitory activities of extracts from aromatic plants used in Mediterranean diet. *J. Food Sci. Technol.* **2017**, *54*, 219–227. [CrossRef]

59. Luo, Y. Alzheimer's disease, the nematode *Caenorhabditis elegans*, and ginkgo biloba leaf extract. *Life Sci.* **2006**, *78*, 2066–2072. [CrossRef]

60. Jivad, N.; Rabiei, Z. A review study on medicinal plants used in the treatment of learning and memory impairments. *Asian Pac. J. Trop. Biomed.* **2014**, *4*, 780–789. [CrossRef]

61. Christen, Y. *Ginkgo biloba* and neurodegenerative disorders. *Front. Biosci.* **2004**, *9*, 3091–3104. [CrossRef]

62. Uysal, S.; Zengin, G.; Locatelli, M.; Bahadori, M.B.; Mocan, A.; Bellagamba, G.; De Luca, E.; Mollica, A.; Aktumsek, A. Cytotoxic and enzyme inhibitory potential of two *Potentilla* species (P. speciosa L. and P. reptans Willd.) and their chemical composition. *Front. Pharmacol.* **2017**, *8*, 290. [CrossRef]